NASA CONTRACTOR REPORT

NASA CR-360

NASA CR-360

BASIC STUDIES ON DISPERSION HARDENING

by Robert Grierson and L. J. Bonis

Prepared under Contract No. NASw-726 *by*
ILIKON CORPORATION
Natick, Mass.
for

NATIONAL AERONAUTICS AND SPACE ADMINISTRATION - WASHINGTON, D. C. - JANUARY 1966

NASA CR-360

BASIC STUDIES ON DISPERSION HARDENING

By Robert Grierson and L. J. Bonis

Prepared under Contract No. NASw-726 by
ILIKON CORPORATION
Natick, Mass.

for

NATIONAL AERONAUTICS AND SPACE ADMINISTRATION

For sale by the Clearinghouse for Federal Scientific and Technical Information
Springfield, Virginia 22151 – Price $3.00

I. SUMMARY

The addition, to a metallic matrix, of a suitably dispersed second phase is one of the most potent methods of increasing the strength of this matrix. In order to obtain a better understanding of the strengthening due to the presence of the second phase, extensive studies into dispersion strengthened alloys have been carried out over a number of years. Initially, these studies centered on the relationship of the observed mechanical properties to the size, shape and distribution of the second phase particles and on the mechanism of interaction of moving dislocations with these particles. Recently, however, strengthening effects which are not directly attributable to the second phase morphology have been observed.[1,2] As an example of such an effect is the behavior of TD nickel when it is alternately cold worked and annealed. It is found that annealing cold worked TD nickel at temperatures which would be expected to give complete recovery of the matrix (e.g., 1300°C) results in an increase in tensile strength (at 1100°C) as compared with the unworked alloy. No change in the properties of the second phase is observed and it is therefore concluded that some change in the behavior of the matrix must have occurred.

It has been observed that, at the annealing temperatures used, the dislocation structure introduced into the matrix by cold work has annealed out and thus that this structure cannot be responsible for the increase in strength. At least two possible strengthening

mechanisms would explain the observed behavior:

1. The retention, after annealing, of some form of substructure other than the dislocation tangles introduced by cold work.
2. The retention of substantial elastic strains in the matrix.

The occurrence of either of these mechanisms is due to the presence of the particles preventing either the substructure or the elastic strains from annealing out in the manner observed in single phased materials.

In the studies being described in this report, two techniques of observation have been used to determine the qualitative and quantitative nature of the substructure and elastic strains retained in cold worked and annealed dispersion strengthened alloys. These techniques are transmission electron microscopy and the Fourier analysis of the profiles of x-ray diffraction lines.

Transmission electron microscopy has been used in two ways - for the normal observation of substructure and for the observation of diffraction effects caused by elastic strains at the particle-matrix interface. X-ray analysis has been used to measure directly the elastic strains in the matrix and also to examine for the existence of various forms of substructure such as stacking faults and twin boundaries.

The transmission electron microscopy observations show that partial annealing out of the dislocation structure introduced by cold work occurs at temperatures as low as 700°C and that it is

completely removed on annealing at 1100°C and above.[3,4] No form of substructure which could be correlated with increased high temperature (1100°C) strength can be observed. Attempts at observing elastic strains associated with the particle-matrix interface were only successful in the case of small ($< 100\text{Å}$) particles in internally oxidized alloys. These strains are thought to be associated with the existence of coherency between the particle and the matrix and are not associated with the working and annealing process.

The x-ray observations did not detect the existence of any substructure in annealed specimens but did show that a high level of elastic strain is retained in cold worked dispersion strengthened alloys. Within the experimental error of the observations, the elastic strain level was found to be approximately constant after annealing cold worked materials at temperatures between 700°C and 1440°C and this strain level was found to be greater than that in unworked material. The largest elastic strains were found to be present in the cold worked alloys.

It is concluded, therefore, that the increase in strength which is observed on alternately cold working and annealing dispersion strengthened alloys is due to the inability of the annealing treatment to relieve all the elastic strains introduced into the matrix by the cold working.

II. TECHNIQUES

A. Transmission Electron Microscopy

1. Interfacial Strain Measurements

When elastic strains are associated with the particle-matrix interface, a diffraction contrast effect can, under certain conditions, be observed.[5-12] Essentially, this contrast effect is in the form of two D-shaped lobes, one on either side of the particle which causes the effect. When one strong reflection is operating, these D-shaped lobes are placed symmetrically about a line of no contrast perpendicular to the reciprocal lattice vector corresponding to the reflection. The contrast effect is visible only when one or more sets of lattice planes diffract strongly and will disappear when the foil is tilted away from this position. The existence of these diffraction effects has been predicted theoretically, on the basis of the dynamical theory of electron diffraction, by Ashby and Brown,[5] and it has been shown[6] how it is possible to calculate the magnitude of the interfacial strains from measurements of the widths of the D-shaped lobes.

There are two types of effect which can cause the type of elastic strains that would lead to the existence of the D-shaped lobe diffraction effect. These two effects are (1) the existence of coherency between the particle and the matrix and (2) the occurrence of differential volume changes between the particle and the matrix. These differential volume changes could occur

because of the difference in coefficient of thermal expansion of the particle and the matrix, due to allotropic phase changes of either the particle or the matrix, or on the formation of the particle within the matrix. D-shaped lobes caused by the occurrence of coherency have been observed in precipitation strengthened alloys by Becher,[7] Bean and Livingston[8] and Phillips and Livingston,[9] and in a dispersion strengthened alloy ($Cu-Al_2O_3$) by Ashby and Smith.[10] In other dispersion strengthened alloys (e.g., $Cu-SiO_2$[10,11] and $Al-Al_2O_3$[12]), the occurrence of the strains producing D-shaped lobes is thought to be due to the difference in thermal expansion coefficient of the two phases. In the case of the $Cu-SiO_2$ alloys, the elastic strains have been calculated to be between 0.1 and 1.0%.

2. Observation of Substructure

The standard techniques of observing thin films, including the use of a tilt stage, were used to observe the substructure of the cold worked and annealed TD nickel.

B. X-Ray Diffraction

The existence of elastic strains and of substructure in a crystalline solid will have an effect on the shape and angular position of x-ray diffraction lines which are obtained by using the crystalline solid as the diffracting medium. The presence of elastic strains in a crystalline solid will cause the interplanar

spacings in the strained material to be different from that in unstrained material. If uniform elastic strains exist throughout a sample, then the interplanar spacings in all regions would be the same, and differ by a quantity Δd from that in unstrained material. This causes a change of $\Delta 2\theta$ in the diffracted angle where the relationship of $\Delta 2\theta$ and Δd can be obtained by differentiating the Bragg equation

$$\lambda = 2d \sin \theta$$

$$\Delta 2\theta = -2\left(\frac{\Delta d}{d}\right) \tan \theta$$

If, however, the existing strains are non-uniform, then these will cause the interplanar spacings in different regions to be different, with the result that the x-rays diffracted by these regions are diffracted through slightly differing angles. The profile of the diffraction line (i.e., the distribution of intensity with diffracted angle) is thus broadened as compared with unstrained material. In general, homogeneous, long range strains (macrostrains) alter the position of x-ray diffraction lines while short range strains alter the profile of these x-ray lines.

Other properties of the material under observation can have an effect on the profile and position of the x-ray diffraction line. These properties are the size of the coherently diffracting domains within the material and the existence of various kinds of lattice faults. The smallness of the coherently diffracting

domains contributes to the shape of the line but not to its position, and the effect on the line profile of the size of the domains can be separated from the strain effects described above by a method which involves the Fourier analysis of the line profiles.[13] The types of lattice faults which will give observable effects are stacking faults[14] and twin boundaries.[15] Their existence causes diffraction line broadening due to their behavior as boundaries of coherently diffracting domains. Their presence can be distinguished from that of other forms of domain boundary because they have additional effects on the diffraction lines. Twin faults cause an assymmetry of the line profile whereas stacking faults cause a shift in the position of the diffraction line.

The experimental observation of the x-ray diffraction lines involves the measurement of the intensity as a function of diffracted angle. The first step in the treatment of the intensity vs. diffracted angle data is to separate the intensity due to the $K\alpha_1$ radiation from that due to the $K\alpha_2$. This was accomplished by using Rachinger's technique.[16] This technique assumes (1) the profile of the $K\alpha_1$ and $K\alpha_2$ components are geometrically similar, (2) the intensity of the $K\alpha_2$ peak is half that of the $K\alpha_1$. The Rachinger separation yields the intensity of the $K\alpha_1$ line as a function of 2θ. To find the peak position from this data, the angular position of points of equal intensity are found and the bisector of these two angles is cal-

culated. A line is drawn through the angular position of the bisectors at different heights and the point where this line intersects the peak profile is used as the peak position. Rachinger's technique is employed because, in the case of cold worked material, it is necessary to separate the $K\alpha_1$ and $K\alpha_2$ components to check accurately the position and assymmetry of the line.

To determine if assymmetry of the peaks exists, the slope of the line drawn through the bisectors is measured. As assymmetry could be caused by effects in the x-ray optics, a similar measurement is carried out using a well annealed pure nickel sample. This will cause no effects due to crystalline imperfection and any difference in slope observed between the pure nickel and the TD nickel samples can be assumed to be due to effects (twins) in the TD nickel.

After the $K\alpha_1$ component of the x-ray line has been analyzed for position and symmetry, a Fourier analysis of the shape of this component is carried out. The method used is a modification of one due originally to Warren and Averbach[13] and it allows us to calculate the size of the coherently diffracting domains and the elastic strains within the specimen under observation. This method will now be described.

The shape of the x-ray diffraction line which we observe is controlled by two factors. One is the x-ray optics of the instrument used to produce and measure the diffraction line in question,

and the other is the degree of crystalline perfection of the material under observation. Departure from perfection in either case will cause an increase in the width of the diffraction line.

When a diffraction line is broadened by two effects, then the variation of intensity, h(x), which we observe across this line is related to the distribution of intensity which we would obtain when only one effect is present (f(x) or g(x)) by an equation of the form:

$$h(x) = f(y)\, g\,(x - y)\, dy \qquad (1)$$

Let us call f(x) the effect of crystalline imperfection and g(x) the x-ray optical effect. We measure h(x) directly and, if we can find g(x), then we can compute f(x). We find g(x) by using a specimen which gives negligible line broadening due to its own imperfection. The calculation of f(x) is carried out in the following way.

The functions f(x), g(x) and h(x) can all be represented by Fourier series of the form:

$$f(x) = \sum_{-\infty}^{+\infty} F_t\, e^{\frac{-2\pi i x^t}{a}} \quad \text{etc.} \qquad (2)$$

By substituting equation (2) into equation (1) and then suitably manipulating the resulting equation, we can obtain F_t in terms of G_t and H_t.

A computer program (Appendix 1) has been written which allows us to calculate G_t and H_t from the measured values of g(x) and h(x). Using these calculated values, we were able to find a set of values of F_t. It is these values of F_t we use to determine the structure within the specimen under observation.

The above is a purely mathematical analysis of the shape of the x-ray diffraction lines. That the values of F_t have a physical meaning has been shown by Warren.[13] In the case under consideration, F_t can be considered as the product of two components, F_t^D and F_t^S. F_t^D is due to the size of the coherently diffracting zones within the sample and F_t^S is due to the presence of elastic strains within the specimen. It has been shown that F_t^D is independent of the order of the diffraction line whereas F_t^S is dependent on the order of the line. We can therefore write:

$$F_t\ (l_o) \;=\; F_t^D\ \ F_t^S\ \ (l_o) \qquad (3)$$

where $l_o = \sqrt{(h^2 + k^2 + l^2)}$ is the order of the line.

Now, it is possible that the crystalline defects we are concerned with may be different in unlike directions through the crystalline lattice. The different diffraction lines contain information about the strains and the domain size in a direction perpendicular to the crystallographic planes causing them. Therefore, any analysis must use lines of different order which are parallel to each other (i.e., a set like the 100, 200, 300).

Thus, to separate the parts of $F_t(l_o)$ due to strains and domain size, we use the Fourier coefficients for a given family of planes. From equation (3):

$$\text{Log } F_t(l_o) = \log F_t^D + \log F_t^S(l_o) \qquad (4)$$

It has been shown that:

$$F_t^S(l_o) \propto e^{\frac{-2\pi^2 \, l_o^2 \, (\varepsilon^2_L) \, L^2}{a^2}}$$

where $\sqrt{(\varepsilon^2_L)}$ is the strain over a distance L in the lattice in the direction under consideration.

Substituting in equation (4):

$$\text{Log } F_t(l_o) = \log F_t^D - \left(\frac{2\pi^2 \, (\varepsilon_L)^2 \, L^2}{a^2}\right) l_o^2 \qquad (5)$$

A plot of $\log F_t(l_o)$ against l_o^2 therefore has a slope of

$$-\frac{2\pi^2 \, (\varepsilon_L)^2 \, L^2}{a^2}$$

The Fourier coefficients $F_t(l_o)$ have been obtained for a series of values t and these values of t are related to the distance L in the above expression by:

$$L = t \cdot d$$

where d is the separation of the planes yielding the diffraction line under consideration and L is a distance in the crystal, perpendicular to these planes.

By considering the variation of $F_t(l_o)$ against t for lines of a given family (e.g., the 100, 200 and 300, etc.) and using the relevant value of d for the lines under consideration, we can obtain the variation of $F_t(l_o)$ versus L. The values of $F_t(l_o)$ are then normalized so that $F_{t=0}(l_o) = 1$ and a plot of $\log F_t(l_o)$ against l_o^2 is made for different values of L. From these we obtain values of

$$\frac{2\pi^2 \ (\epsilon_L)^2 \ L^2}{a^2}$$

as a function of L and thus can find $\sqrt{\epsilon^2}_L$ as a function of L.

Also, from a plot of $\log F_t(l_o)$ against l_o^2 we can find $\log F_t^D$ by measuring the intercept of this plot with the line $l_o = 0$. This again is obtained as a function of L. If, using these values of $\log F_t^D$, we plot F_t^D against L and extrapolate the values obtained to $F_t^D = 0$, then the intercept with the L axis gives us the size of the coherently diffracting domains.

III. EXPERIMENTAL METHODS

A. Transmission Electron Microscopy Studies of Interfacial Strain

During the first year of this research program[17] it was observed that D-shaped lobes could only be detected when very fine particles were observed and, for this reason, it was thought that they must be caused by coherency strains.

Research in this field has been continued into three alloys. One, DuPont's TD nickel, was obtained commercially and the other two, Ni + Al_2O_3 and Ni + Cr_2O_3, were fabricated at Ilikon. The purpose of the Al_2O_3 and Cr_2O_3 containing alloys was to give material which contained fine particles and thus would be more apt to show coherency strains. The Ni + Al_2O_3 alloy was fabricated by the internal oxidization, at 750°C, of a nickel + 1/2% aluminum solid solution powder. This powder was then compacted and extruded to give 3/8" diameter rod. The Ni + Cr_2O_3 alloy was fabricated by the internal oxidization, at 800°C, of .004" thick foils of a nickel + 1% chromium alloy. In all three cases, the oxide content was approximately 2 vol. %.

Foils which were to be thinned for observation were obtained from the Ni-ThO_2 and Ni-Al_2O_3 rods by cutting .05" thick slices, chemically polishing these to .045" and then rolling them to .010". Various heat treatments were then given to the foils prior to their thinning down for observation in the electron microscope.

A modified Bollman technique was used to prepare thin films from the foils. This technique, having three separate steps, is illustrated diagrammatically in Figure 1. Initially, the two point electrodes are placed at a distance of approximately 3/4" from the foil, which is then polished more or less uniformly down to a thickness of approximately .004". Two small, tightly fitting plastic tubes are then placed over the unshielded tips of the electrodes and the electrodes are then bent so that the open end of these shields touch the foil directly opposite each other. The tips of the electrodes are within 1/8" of the foil. Polishing is then continued and a pair of shallow indentations are obtained on the foil. This procedure is repeated at several places on the foil. The rest of the foil continues to polish at a very slow rate. After these indentations have been formed, the original electrode geometry is resumed and the electrolyte temperature is lowered to the range $-15^{\circ}C$ to $-20^{\circ}C$. Polishing is then continued until small holes appear at the indentations. Material to be viewed is then cut from these regions and from the bridges which form between neighboring holes. This somewhat elaborate technique yields foils which have large thin areas and thus allowed the observation of more usable material in any one specimen preparation.

The electrolyte used for thinning was a mixture of 40 vol. % H_3PO_4, 35 vol. % H_2SO_4 and 25 vol. % H_2O.

The thin foils thus obtained were placed in the tilting stage of an Hitachi HU-11 microscope. Two techniques were used

in attempts at observing the D-shaped lobes. First, observation of the foil by electron diffraction was carried out initially and the foil was tilted until one set of lattice planes was diffracting strongly. This is the optimum condition for the observation of the diffraction contrast effect. The area of interest was then viewed by transmission in order to determine the nature of D-shaped lobes present, if any. The other technique of observation, electron diffraction was not used and given areas of the foil were observed while they were slowly tilted through a range of orientation.

B. The Observation of Substructure

The thin foils which were used in the observation of the effect of annealing on cold worked TD nickel were prepared in a similar manner to that already described. The only difference was that all foils were prepared so that their rolling direction always had the same relationship to the extrusion direction of the TD nickel rod. This relationship is shown in Figure 2.

The observation of these foils was carried out using the tilt stage of the electron microscope.

C. X-Ray Diffractometry

Rectangular blocks approximately $1\frac{1}{2}$" x 3/8" x 3/8" were cut from the as obtained rod. These were then rolled in the direction shown in Figure 2 to a thickness of approximately .085" and the two largest surfaces were ground flat. The plate of TD nickel

thus obtained was then given the required treatment. The surface to be examined was reground and polished mechanically. In the final polish, 0.05μ particle size alumina was used. The work layer produced by this final polish was then removed by chemical polishing, at 85°C, using a mixture of 30% nitric acid, 10% phosphoric acid, 10% sulphuric acid and 50% acetic acid. The surface thus obtained was bright, flat and did not contain any disturbance due to the polishing.

The diffraction line profiles were measured with an automated Picker bi-plane x-ray diffractometer. A special specimen holder was designed and built to allow a more accurate and reproducible positioning of the specimen. The line profiles were determined by carrying out intensity measurements at intervals of either 1/30° or 1/60° over a range of 3° on both sides of the nickel peaks of interest to us. In order to carry out the separation of the x-ray optical and specimen induced line broadening, pure nickel, annealed for 1 hour at 800°C, was used as standard, so-called "defect free" specimen.

IV. RESULTS

A. Strains at the Particle-Matrix Interface

The Ni-ThO_2, Ni-Al_2O_3 and Ni-Cr_2O_3 specimens were all examined for the presence of D-shaped lobes. The only D-shaped lobes which were observed were associated with very fine ($<100\text{Å}$) particles in the Ni-Al_2O_3 system (Figure 3). Even though particles of a similar size existed in the Ni-Cr_2O_3 alloy (Figure 4), we have not detected D-shaped lobes associated with them. Observation of thin foils which had been water quenched from temperatures up to 900°C showed that this treatment failed to introduce D-shaped lobes into the Ni-ThO_2 and did not either increase the number or the magnitude of the lobes in the Ni-Al_2O_3 alloy. Cold working and annealing these alloys was not observed to have any effect on either the number or the size of the D-shaped lobes. Because of the difficulty in seeing and measuring the D-shaped lobes in the Ni-Al_2O_3 system, no attempt has been made to calculate the strains associated with them.

B. Transmission Electron Microscopical Observation of the Substructure of TD Nickel

The substructure of the as received TD nickel is shown in Figure 5. This material had been formed by extrusion and had then been swaged to give the 1/2" diameter received by Ilikon. Prior to our receiving it, the 1/2" diameter rod had been given a stress relieving anneal at 1010°C. The microstructure of this material shows it to be free of heavy dislocation tangles but it does have a comparatively small substructural unit which has an

elongated shape - the longer axis presumably being the direction of elongation during extrusion and swaging.

Cold working this material introduces the heavy dislocation structure shown in Figure 6. This structure is mainly composed of dislocation tangles although some evidence of the formation of a cell structure can be observed. This cell structure is not as well defined as that in pure nickel which has received the same treatment (Figure 7 - upper micrograph). On annealing the cold worked TD nickel at 700°C (Figure 8) or 800°C (Figure 9), some of the dislocation tangles anneal out and the dislocation density of the material can be observed to decrease. The change is not as drastic as that observed for pure nickel (Figure 7 - lower micrograph) which has received the same treatment. In this case, recrystallization occurs and the dislocation substructure is completely removed. On increasing the annealing temperature of the TD nickel to 900°C, a greater change is observed as compared with the 700°C and 800°C anneals. Most of the dislocation tangles anneal out but the matrix still appears to be heavily distorted (Figure 10). Annealing at 1100°C and 1440°C, however, leads to a matrix which apparently retains virtually none of the substructural features which had been introduced by cold working (Figures 11 and 12). Occasional twin boundaries can be observed, but there is no form of substructure which could explain the strengthening reported by other observers.[1,2]

C. X-Ray Diffraction

TD nickel in the following conditions was examined by using

the Fourier analysis of x-ray diffraction lines:

(1) As received.

(2) Cold worked.

(3) Cold worked and then annealed for 1 hour at 700°C.

(4) Cold worked and then annealed for 1 hour at 900°C.

(5) Cold worked and then annealed for 1 hour at 1100°C.

(6) Cold worked and then annealed for 1 hour at 1440°C.

All these specimens had a very strong preferred orientation. Diffraction lines from the ⟨111⟩ family of planes could not be detected whilst those from the ⟨200⟩ and ⟨220⟩ were very strong as compared with the same lines obtained from a pure nickel specimen.

That complete recovery of the matrix does not occur on annealing can be seen by examining the 200 diffraction lines shown in Figures 13-18. Cold worked TD nickel (Figure 13) and pure nickel (Figure 14) give similar line profiles. The effect of annealing the cold worked pure nickel at 700°C is to cause the line profile to become that which would be expected from a well annealed material - the separation of the α_1 and α_2 components being obvious (Figure 15). However, treating TD nickel in the same way does not cause very much change in the line profile (Figure 16) as compared with the cold worked material (Figure 13). When the annealing temperature is raised to 1440°C (i.e., within 15°C of the melting point), the nickel matrix of TD nickel still gives diffraction line profiles of the type to be expected from

cold worked materials rather than annealed materials (Figure 17) and, in fact, the line profile is very similar to that obtained when the material annealed at 700°C (Figure 16) is examined. The line profile of the as received material (Figure 18) shows slightly less broadening than those of any of the cold worked and annealed specimens but it still has the shape which would be expected from a cold worked rather than an annealed material. The qualitative observation of the profiles of the various diffraction lines indicates that the least broadening occurs with the as obtained material, the most with the cold worked material, and that an intermediate level of broadening exists for the cold worked and annealed material. Cold working TD nickel, therefore, induces line broadening which can only be partially annealed out. As will be shown below, this broadening is caused by the existence of elastic strains within the TD nickel. The next step is to carry out an analysis of the position and symmetry of the diffraction lines and then to carry out the Fourier analysis of the line profiles.

Due to the preferred orientation of the TD nickel, only three diffraction lines were strong enough to allow us to carry out sensible intensity vs. diffracted angle measurements. Since we need two lines of the same family in order to be able to carry out the Fourier analysis, we only measured the 200 and 400 lines. The first information to be obtained from the measured data was the position and symmetry of the diffraction lines under consideration. In order to be able to make these measurements accurately,

we had to separate the $K\alpha_1$ and $K\alpha_2$ components. When this was carried out, it was found that, within the experimental error, no difference in symmetry or line position existed between the pure nickel standard and any of the TD nickel specimens.

Using the computer, the Fourier analysis of the line profiles is then carried out. Figures 19 and 20 show typical Fourier coefficient F_t vs. t data. The t axis used with this data is then adjusted to give L values (L = t . d, where d is the relevant interplanar spacing) and the values of log $F_t(l_o)$ are found for different values of L for both the 200 and 400 lines. These values are then plotted against l_o^2 for various distances (L) (Figures 21-26). The slope of this plot is a measure of the elastic strains in the material whilst the intercept with the log $F_t(l_o)$ axis is a measure of the size of the coherently diffracting domains. The line log $F_t(l_o)$ = 0 represents the case of no strain and very large coherently diffracting domains. It can be seen that in all cases elastic strains exist and that the size of the coherently diffracting domains is not very large.

The slopes of the above plots are then used to calculate the variation of elastic strain with distance through the crystal in a direction perpendicular to the 200 and 400 planes. Figure 27 shows this data for the six specimens observed. It can readily be seen that these strains are largest in the cold worked material, at an intermediate level in the cold worked and annealed material and lowest in the as received material. It can also be seen that

varying the annealing temperature within the range 700-1440°C has little or no effect on these elastic strains.

The intercepts with the log $F_t(l_o)$ axis of the lines shown in Figures 21-26 are then used to calculate the size of the coherently diffracting domains within the matrix of the TD nickel. As shown in Figure 28, these were found to be approximately 190Å in the cold worked material and in the range of 500-600Å in the cold worked and annealed material. In the as received material, the domain size was observed to be much larger than in any of the other specimens and, in fact, it is so large that an accurate measurement of it cannot be made. The domain size measurements, therefore, also show that the as received material has the greatest degree of crystalline perfection, that the cold worked material has the least and that the cold worked and annealed material is in an intermediate state. The domain size in the cold worked and annealed material is found to be independent of annealing temperature within the range 700°C - 1440°C.

V. DISCUSSION

The transmission electron microscopy observations of cold worked and annealed TD nickel showed that the heavy dislocation structure introduced during the cold working can be partially annealed out at temperatures as low as 700°C and virtually completely annealed out on annealing at 1100°C. In the specimens annealed at 1100°C and 1440°C, the only substructure observed, occasional twin boundaries, could not account for the increase in high temperature strength which has been observed to result from cold working and annealing.

The important information which has been obtained in these studies is contained in the x-ray data. As a first step in interpreting the meaning of the x-ray observations, it is necessary to consider exactly what is being measured when we talk of elastic strains and coherently diffracting domains. The coherently diffracting domain size which we have measured is a measurement of an average distance in a direction perpendicular to the 200 and 400 planes. Within these domains the crystalline perfection is of a high enough order to allow the coherent diffraction of x-rays to occur. Outside of these domains the atomic planes are not sufficiently in register with those inside the domain for coherent diffraction to occur. The domain boundaries can thus be regarded as regions in which comparatively large deviations from crystalline perfection occur. The strains which we measure are strains within these coherently diffracting domains. When it is said that, for example, $\sqrt{\epsilon^2}_{L=50\text{Å}} = .0035$, we mean that, in an average domain if we start on any plane of atoms and measure perpendicular to it, then the crystal at a distance of 50Å from it will be displaced on average by a strain of .0035 from the position it would have in an unstrained, perfect crystal.

The boundaries between the domains represent some form of disruption of the crystalline lattice which is greater than the elastic strains which we have measured within the domains.

Table 1 compares the values of $\sqrt{\epsilon^2}_{L=50\text{Å}}$ which we have obtained for TD nickel with values of $\sqrt{\epsilon^2}_{L=50\text{Å}}$ obtained by other research groups on other alloys. These alloys have been heavily cold worked at liquid nitrogen temperature before being annealed at low homologous temperatures ($< \frac{1}{2} T_m$).

Material	$\sqrt{\epsilon^2}_{L=50}$
Silver, annealed 5 mins. at 30°C[16]	.0040
Silver, annealed 5 mins. at 100°C[16]	.0015
Copper, annealed 5 mins. at -100°C[17]	.0030
Copper, annealed 5 mins. at 50°C[17]	.0008
90-10 Brass, annealed 20 mins. at 20°C[17]	.0030
90-10 Brass, annealed 20 mins. at 220°C[17]	.0008
Aluminum, annealed 5 mins. at -150°C[18]	.0035
Aluminum, annealed 5 mins. at 25°C[18]	.0010
TD Nickel, as obtained	.0010
TD Nickel, cold worked at 25°C	.0033
TD Nickel, c.w., annealed 1 hr. at 1440°C	.0023

Table 1

It can be seen that cold working TD nickel introduces elastic strains which are of similar magnitude to those found in other

materials which have been heavily deformed. In other materials, however, these strains can be considerably reduced by annealing at temperatures of less than half the melting point of the material, whereas in TD nickel the strains do not undergo as large a reduction even on annealing at temperatures within 15°C of the melting point. This retention of strain is even more obvious when the data for as obtained TD nickel is compared with that for the cold worked and annealed material (Figure 27).

A similar effect is observed when the size of the coherently diffracting domains in TD nickel is compared with those observed in other materials. This data is given in Table 2.

Material	Domain Size
Silver, annealed 5 mins. at 30°C(18)	100Å
Silver, annealed 5 mins. at 100°C(18)	600Å
Aluminum, annealed 5 mins. at -150°C(18)	220Å
Aluminum, annealed 5 mins. at 25°C(18)	630Å
Nickel, annealed at 200°C(19)	400Å
Nickel, annealed at 400°C(19)	400Å
Nickel, annealed at 800°C(19)	2200Å
TD Nickel, cold worked	190Å
TD Nickel, as received	>1000Å
TD Nickel, c.w., annealed 1 hr. at 1440°C	600Å

Table 2

The domain size in cold worked TD nickel is small and similar to that found in other materials which have been heavily cold worked. Annealing the TD nickel at 1440°C causes some increase in the domain size but the change which occurs is not as large as that observed in other materials. On comparing TD nickel in the as received condition with TD nickel which has been cold worked and then annealed at 1440°C, we find that the cold working operation has caused a reduction in the coherently diffracting domain size and that this change is not completely reversed on annealing.

The existence of considerable elastic strains and of a small coherently diffracting domain size indicates that the lattice in cold worked and annealed TD nickel is considerably distorted. This lattice distortion explains the increase in strength obtained when TD nickel is cold worked and then annealed. The response of the matrix of TD nickel to annealing is obviously very different to that of, for example, pure nickel. In a single phased material, the removal of the heavy dislocation structure introduced by cold working leaves behind a comparatively undistorted lattice structure. In TD nickel this is not the case. Although the presence of the particles raises the minimum temperature at which the dislocation tangles will anneal out of the nickel matrix, it does not prevent this from occurring. The presence of the particles, however, does act to "lock" into the lattice a certain amount of elastic strain.

The effect of lattice distortions on the mechanical properties of dispersion strengthened alloys is very important in as far as it provides a strengthening mechanism which continues to be operative at temperatures approaching the melting point of the matrix. A better understanding of ways in which a build up of these distortions can be achieved would help towards the optimization of the properties of dispersion strengthened alloys. It will probably be found that a complex thermal and mechanical treatment is necessary in order to achieve this end. The Fourier analysis of x-ray diffraction lines is important since it would appear to be the only direct technique for the observation of these lattice distortions.

The study currently being reported has only been able to touch on a small corner of the total field which requires consideration. Among the factors which should receive further attention are:

(1) The effect of several alternate cold working and annealing treatments.

(2) The effect of the nature of deformation processes used during cold working.

(3) Orientation effects - TD nickel being an extruded material is very anisotropic.

REFERENCES

1. M. von Heimendahl and G. Thomas, Trans. Met. Soc. AIME 1964, vol. 230, pp. 1520-28.

2. M. C. Inman, K. M. Zwilsky and D. H. Boone, ASM Trans. Quart. 1964, vol. 57, pp. 701-13.

3. J. E. White and R. D. Carnahan, Trans. Met. Soc. AIME 1964, vol. 230, pp. 1298-1306.

4. G. S. Doble and R. J. Quigg, Trans. Met. Soc. AIME 1965, vol. 233, pp. 410-15.

5. M. F. Ashby and L. M. Brown, Phil. Mag. 1963, vol. 8, p. 1083 and p. 1649.

6. M. F. Ashby and L. M. Brown, Fifth International Congress for Electron Microscopy, Vol. 1, Paper K5. Published by Academic Press, 1962.

7. J. J. Becher, Trans. Met. Soc. AIME 1957, vol. 209, p. 59.

8. C. P. Bean and J. D. Livingston, J. App. Phys. 1959, vol. 30, p. 1205.

9. V. A. Phillips and J. D. Livingston, Phil. Mag. 1962, vol. 7, p. 969.

10. M. F. Ashby and G. C. Smith, J. Inst. Met. 1962-63, vol. 91, pp. 182-87.

11. M. F. Ashby, Fifth International Congress for Electron Microscopy, Vol. 1, Paper K6. Published by Academic Press, 1962.

12. R. S. Goodrich and G. S. Ansell, Trans. Met. Soc. AIME 1964, vol. 230, pp. 1372-77.

13. Reviewed in "X-Ray Studies of Deformed Metals", B. E. Warren, Progress in Metal Physics (1959) vol. 8, p. 147.

14. M. S. Paterson, J. App. Phys. 1952, vol. 23, p. 805.

15. J. B. Cohen and C. N. J. Wagner, J. App. Phys. 1962 vol. 33, pp. 2073-77.

16. F. R. L. Schoening and J. N. van Niekerk, Acta Met. 1955, vol. 3, pp. 10-13.

17. C. N. J. Wagner, Acta Met. 1957, vol. 5, pp. 427-34.

18. C. N. J. Wagner, Acta Met. 1957, vol. 5, pp. 477-82.

19. D. Mitchell and F. D. Haig, Phil. Mag. 1957, vol. 2, pp. 15-31.

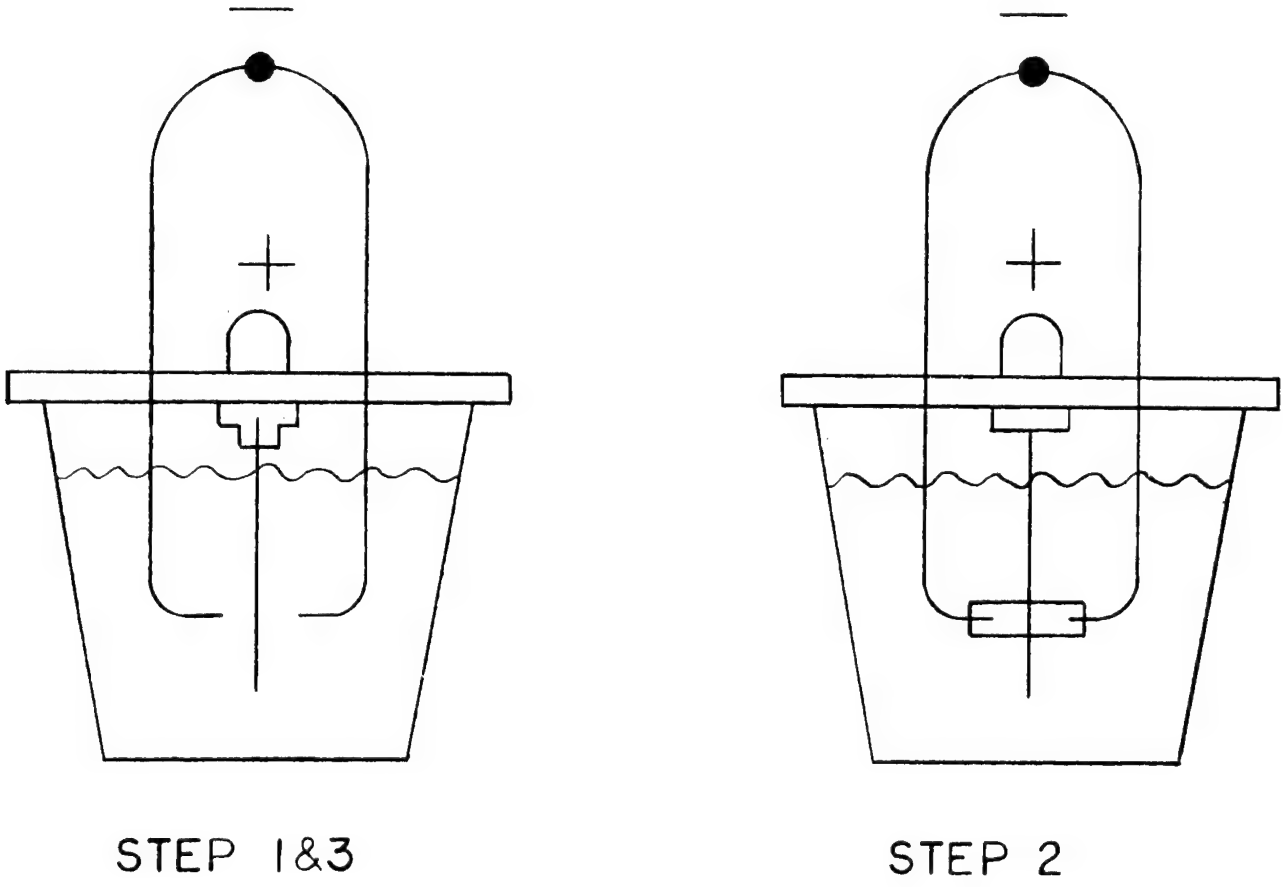

Figure 1. The electrode positions used in the preparation of thin foils

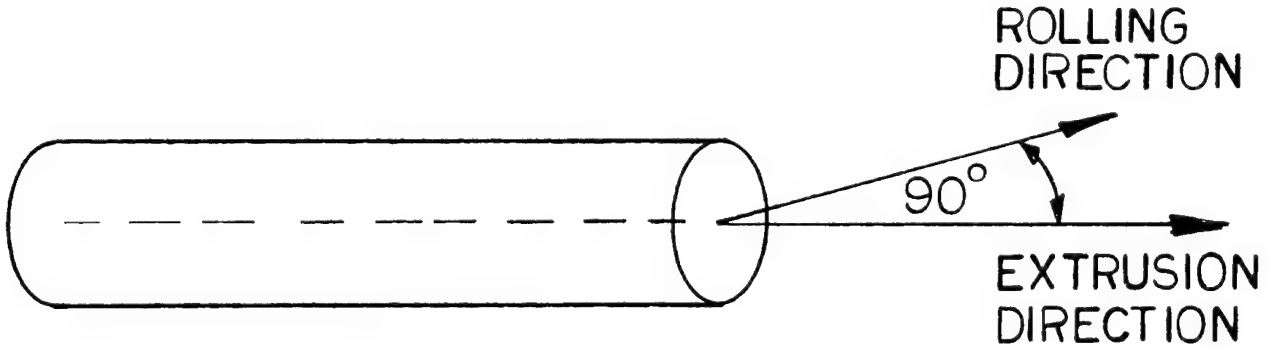

Figure 2. The rolling direction used in the preparation of electron microscopical and x-ray specimens

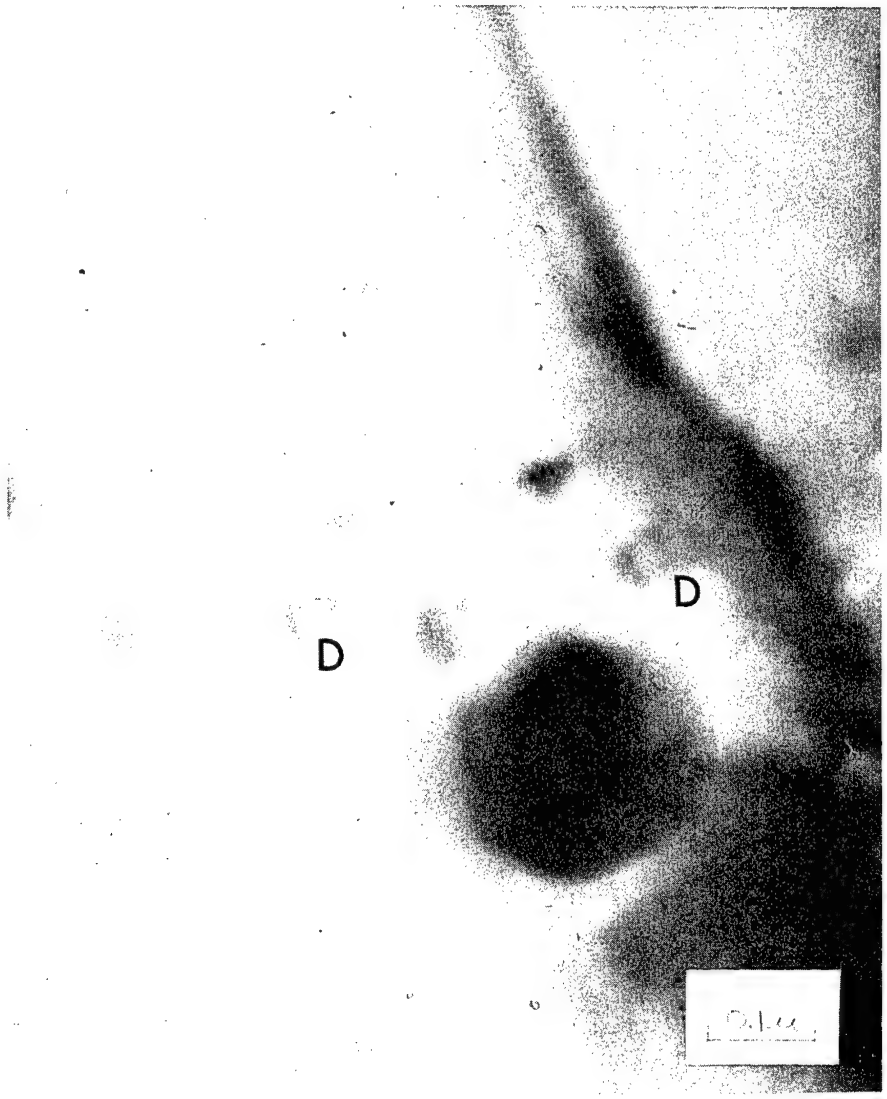

Figure 3. D-shaped lobes in Ni-Al_2O_3 shown at the positions marked D

Figure 4. Ni + 1% Cr alloy after internal oxidization at 800°C

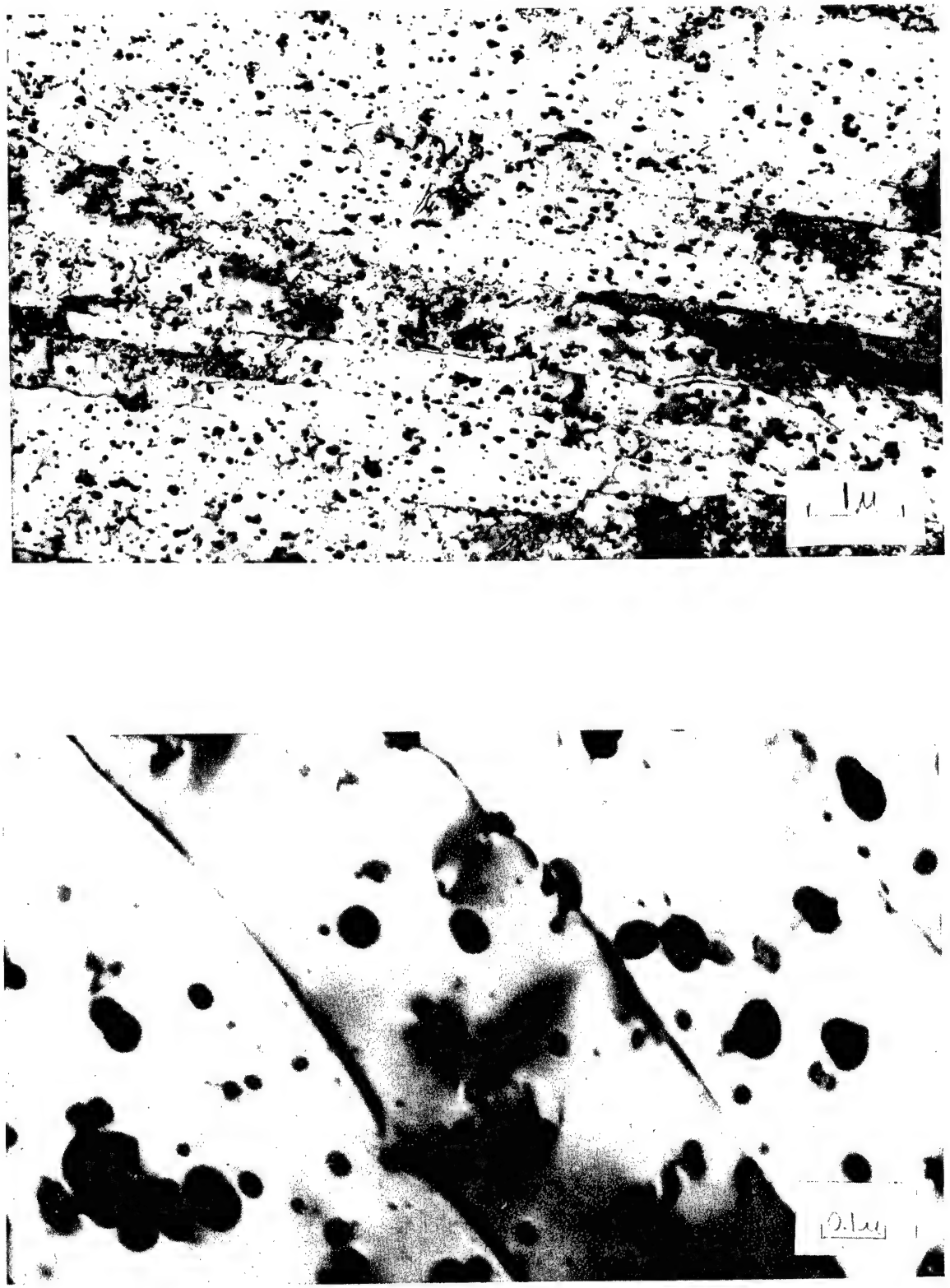

Figure 5. As extruded, TD nickel

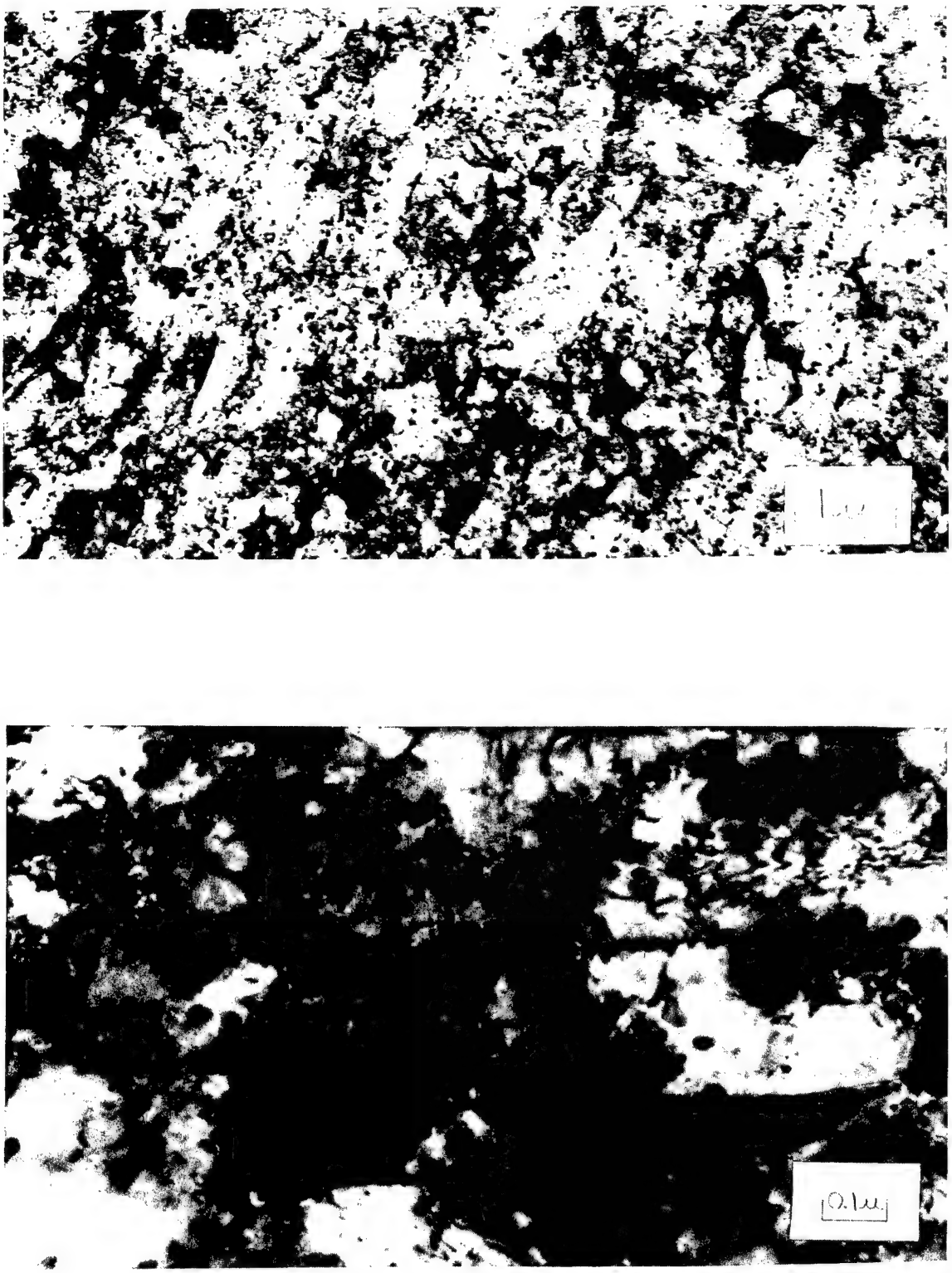

Figure 6. Cold worked, TD nickel

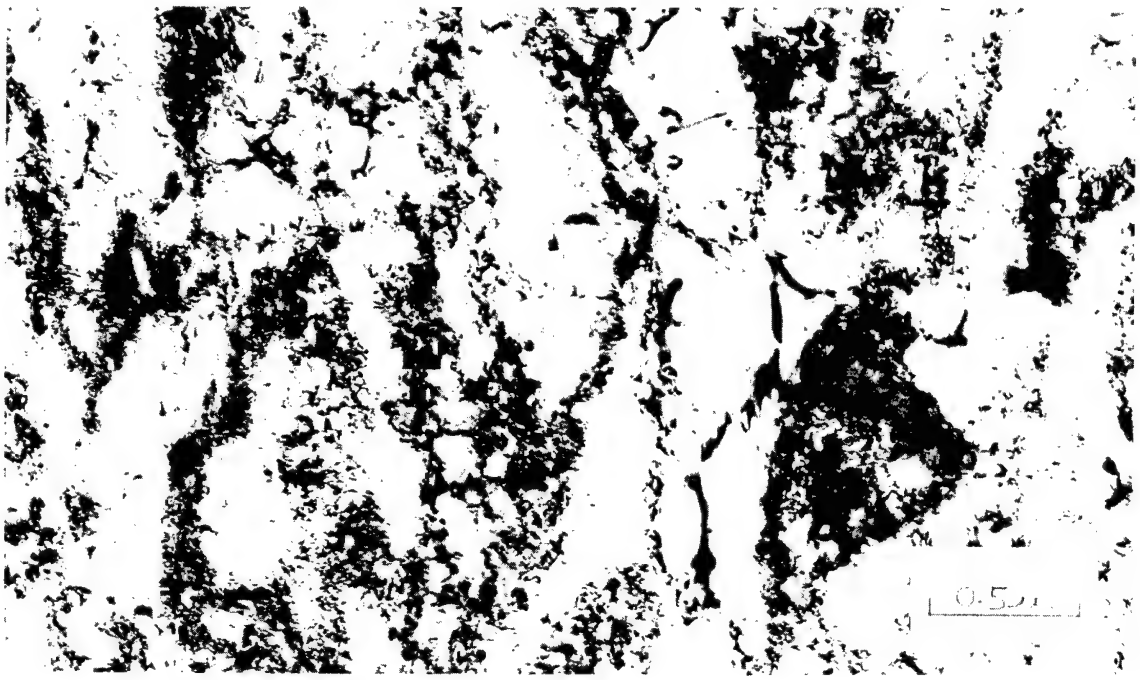

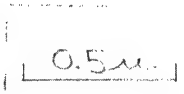

Figure 7. Upper: Cold worked, pure nickel

Lower: Pure nickel, cold worked and annealed at 700°C for 1 hour

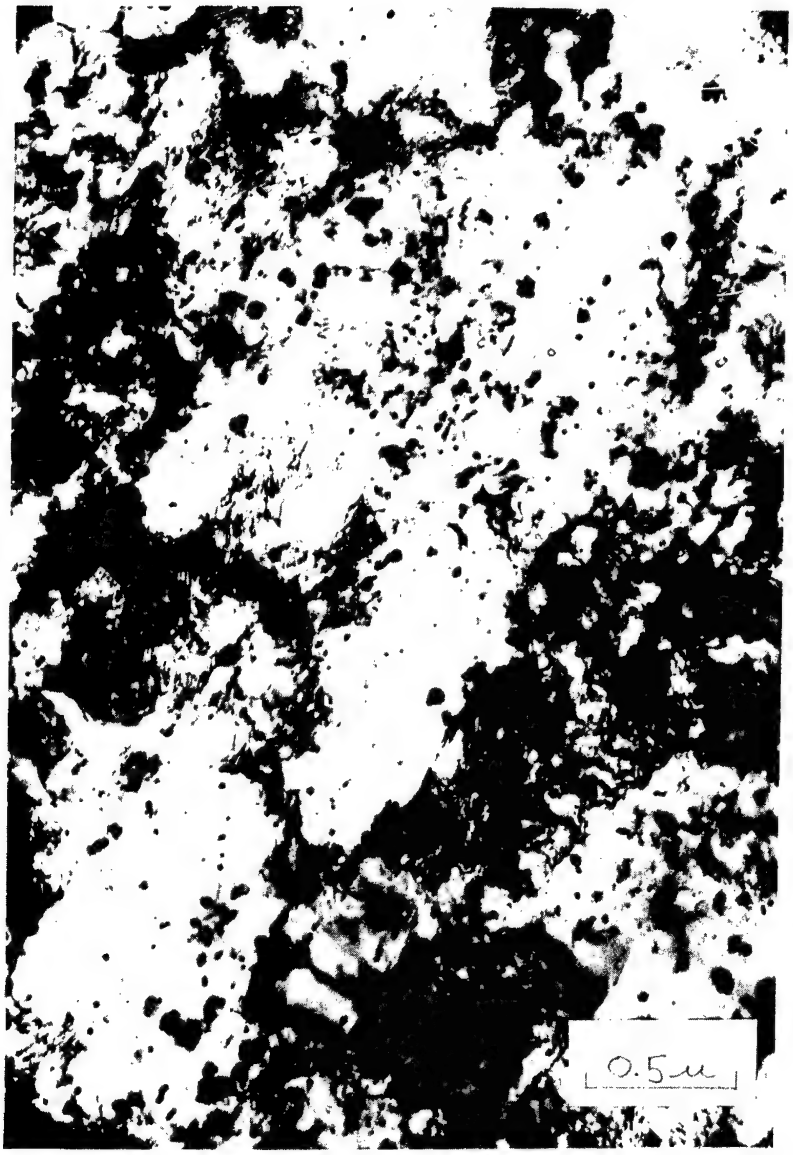

Figure 8. TD nickel. Cold worked and then annealed for 1 hour at 700°C

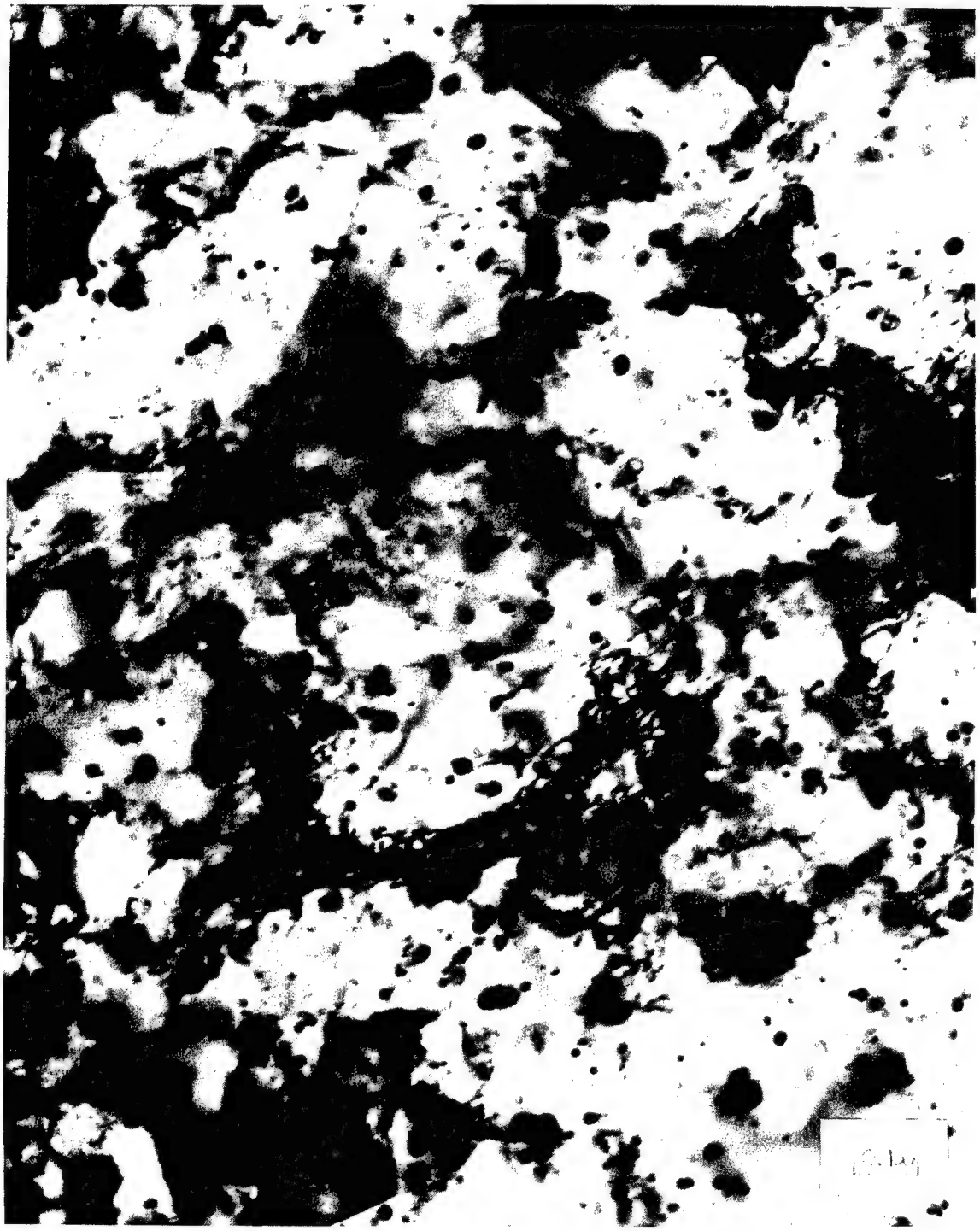

Figure 9. TD nickel. Cold worked and then annealed for 1 hour at 800°C

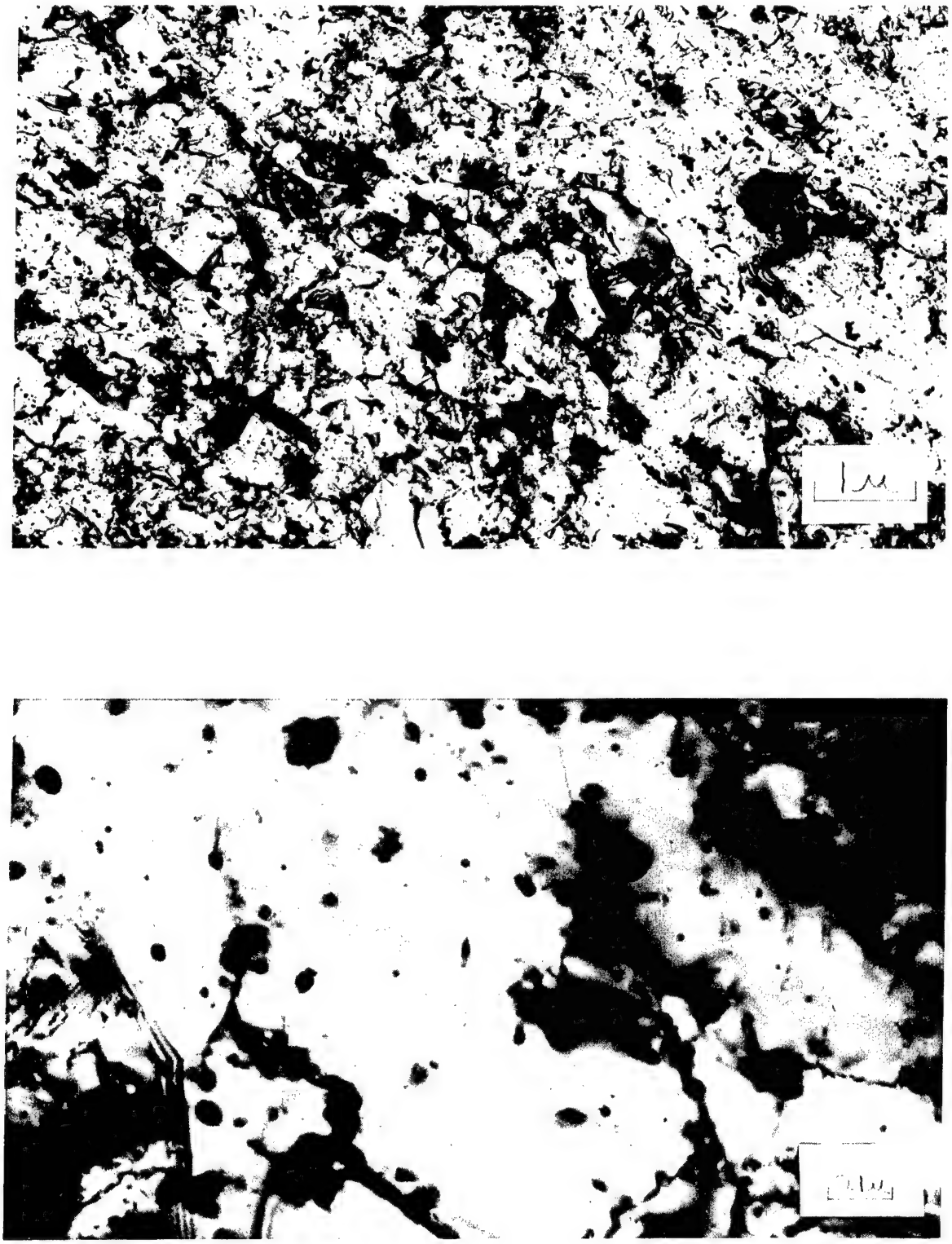

Figure 10. TD nickel. Cold worked and then annealed for 1 hour at 900°C

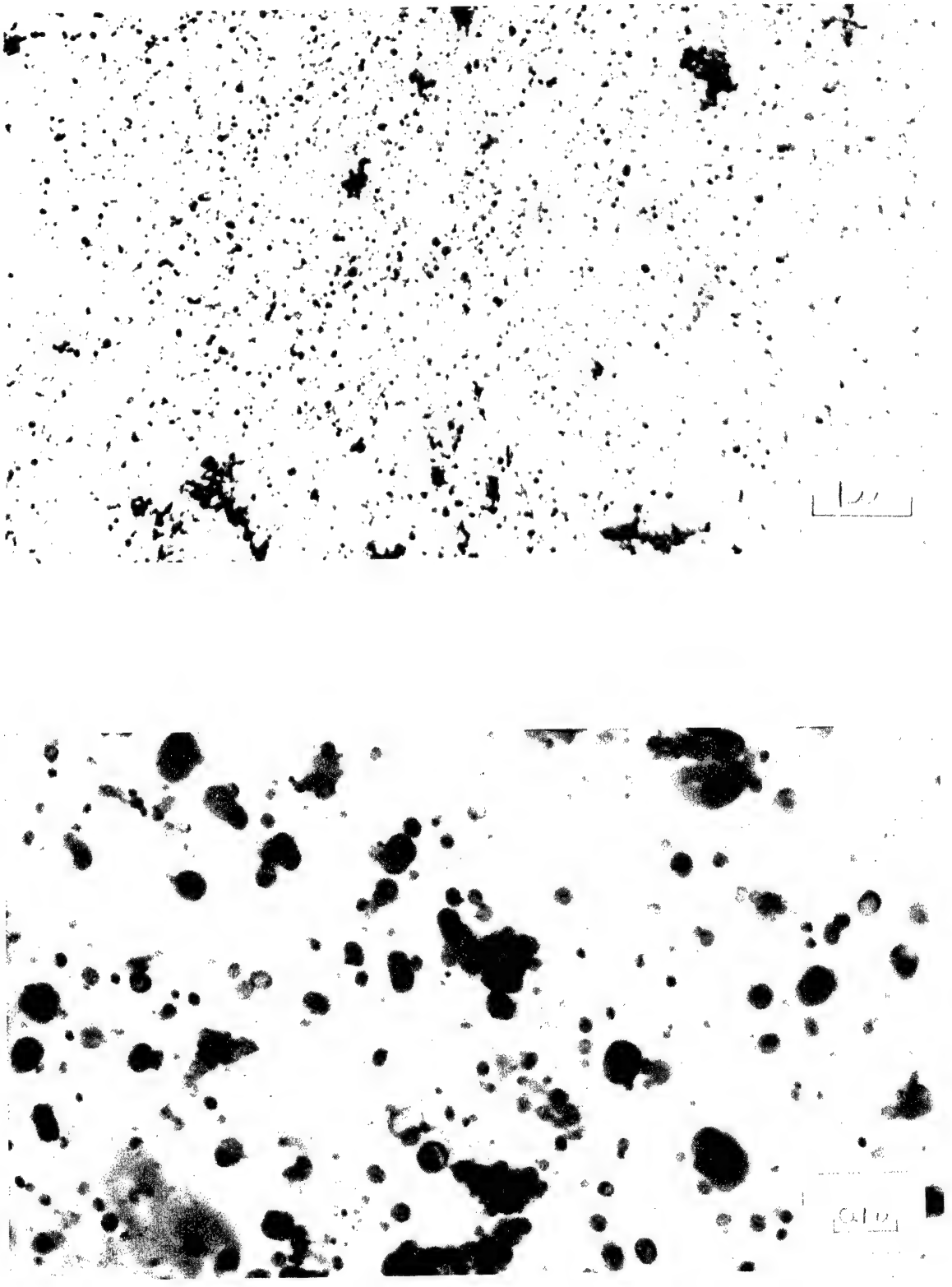

Figure 11. TD nickel. Cold worked and then annealed for 1 hour at 1100°C

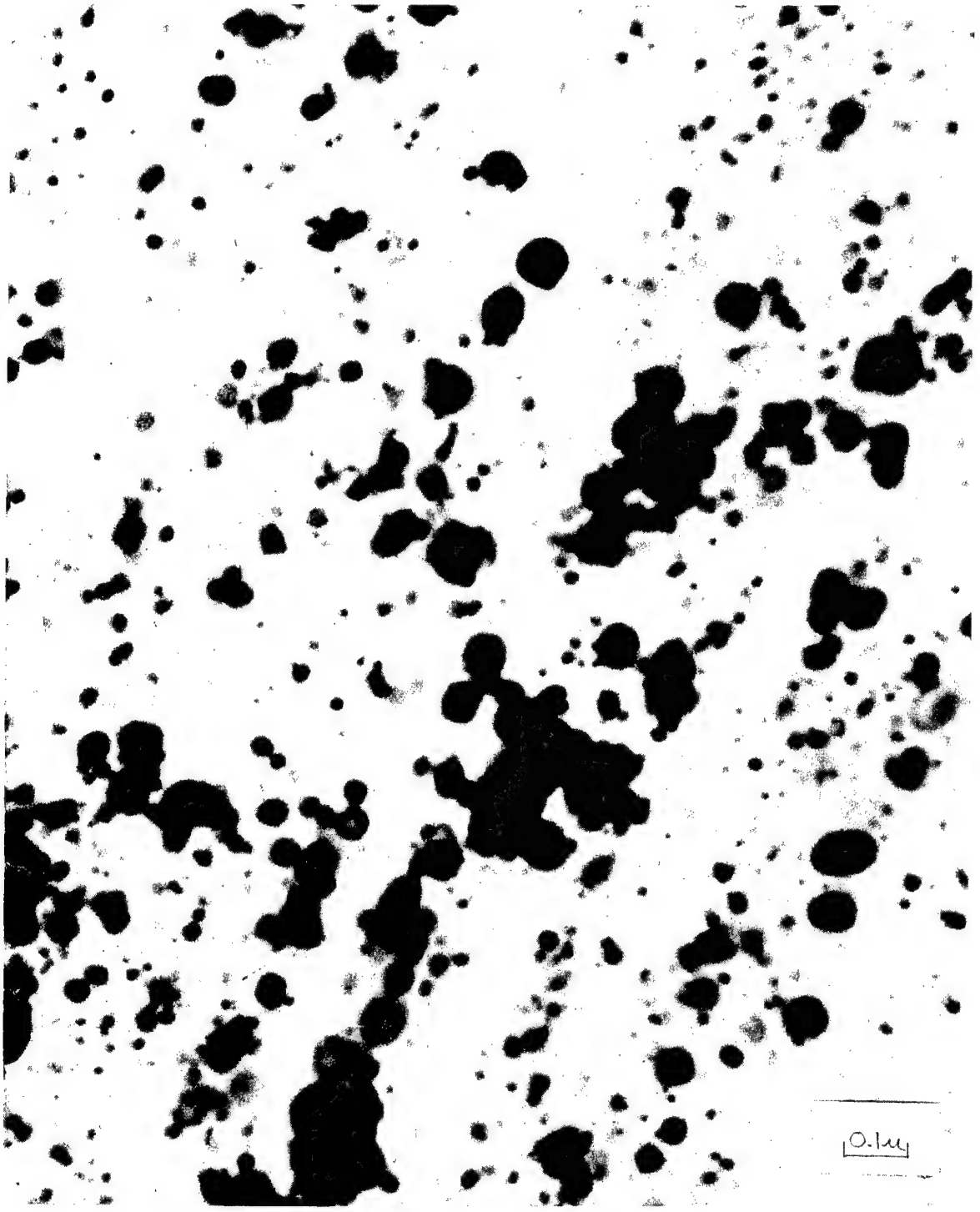

Figure 12. TD nickel. Cold worked and then annealed for 1 hour at 1440°C

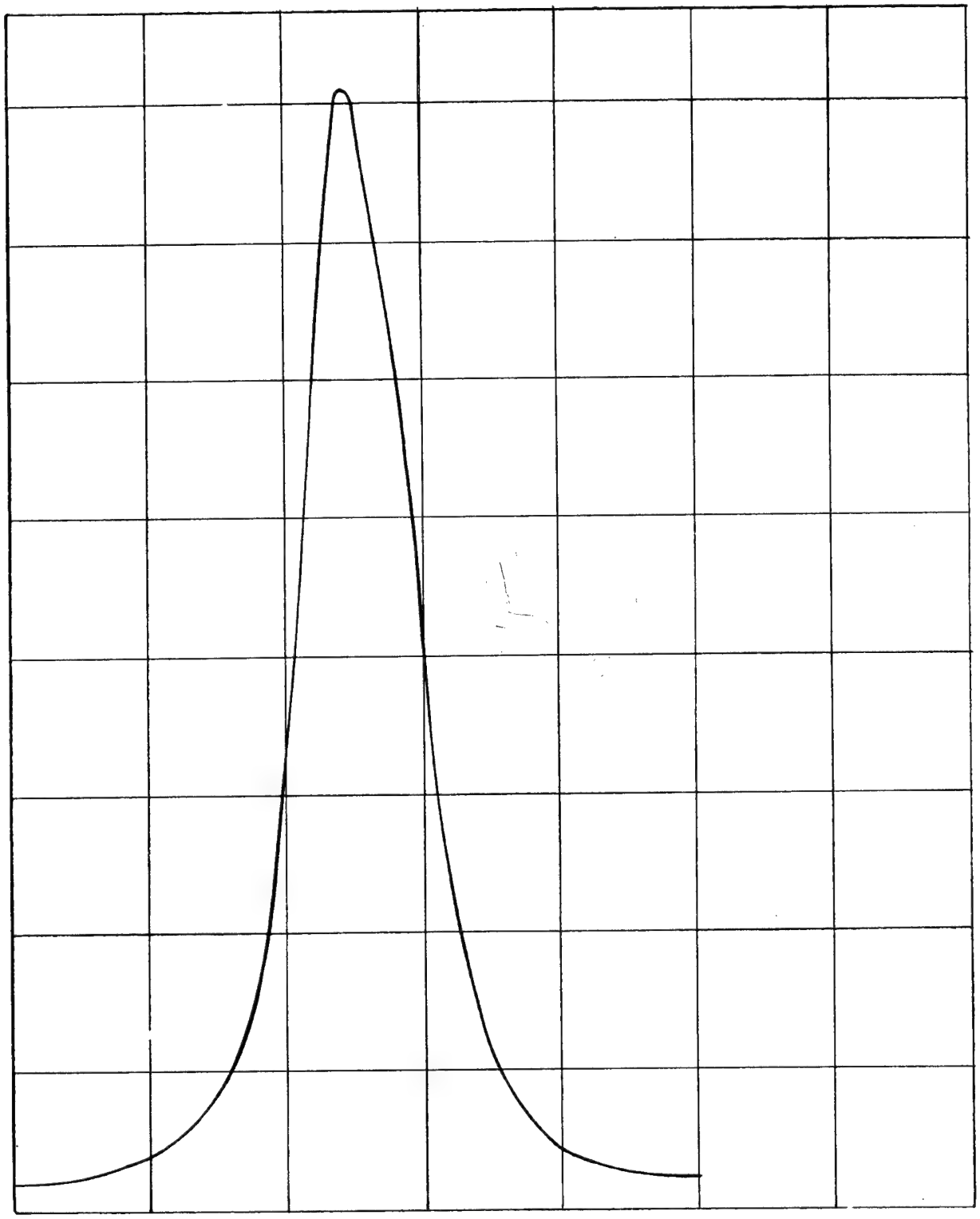

Figure 13. The 200 x-ray diffraction line obtained from cold worked TD nickel

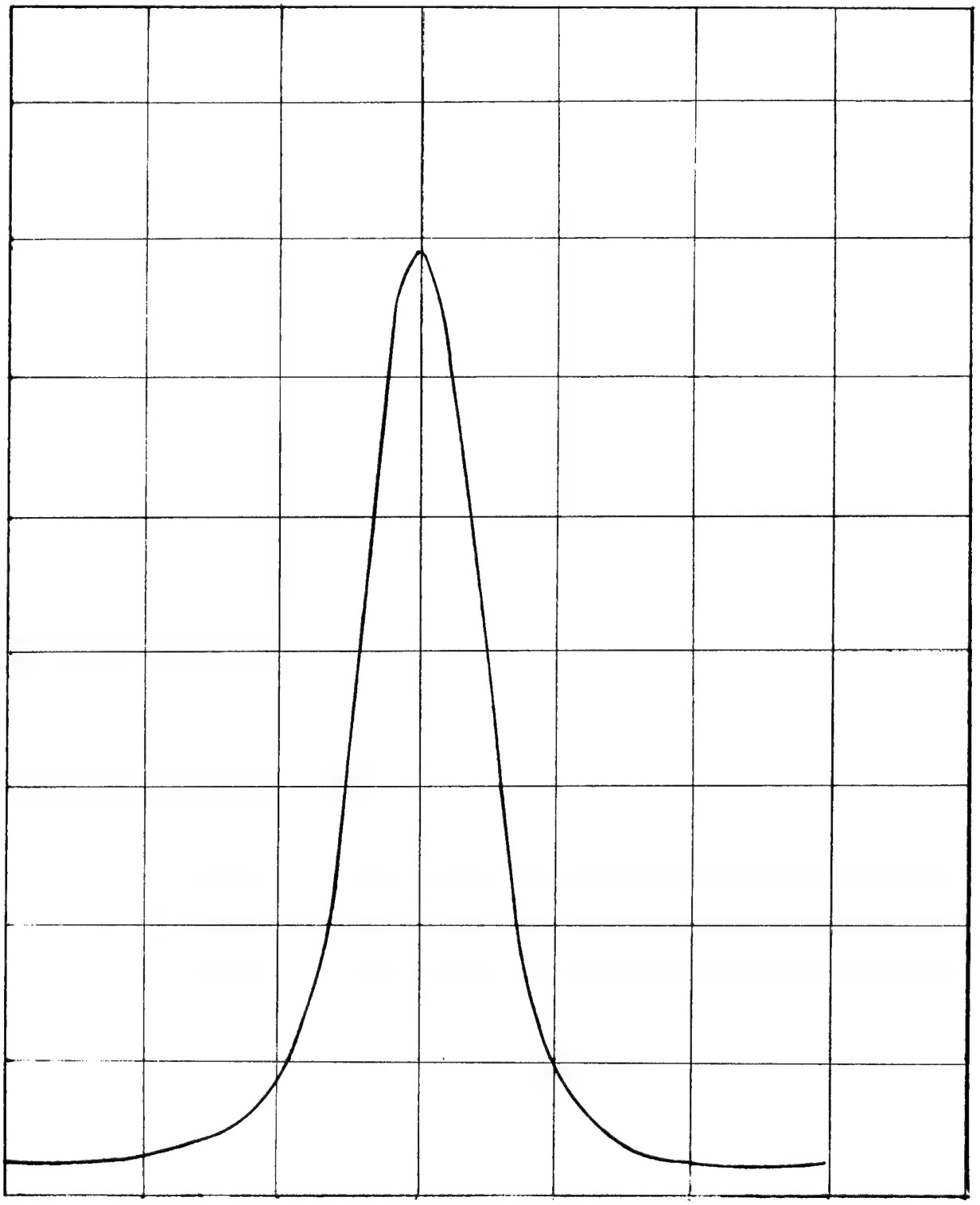

Figure 14. The 200 x-ray diffraction line obtained from cold worked pure nickel

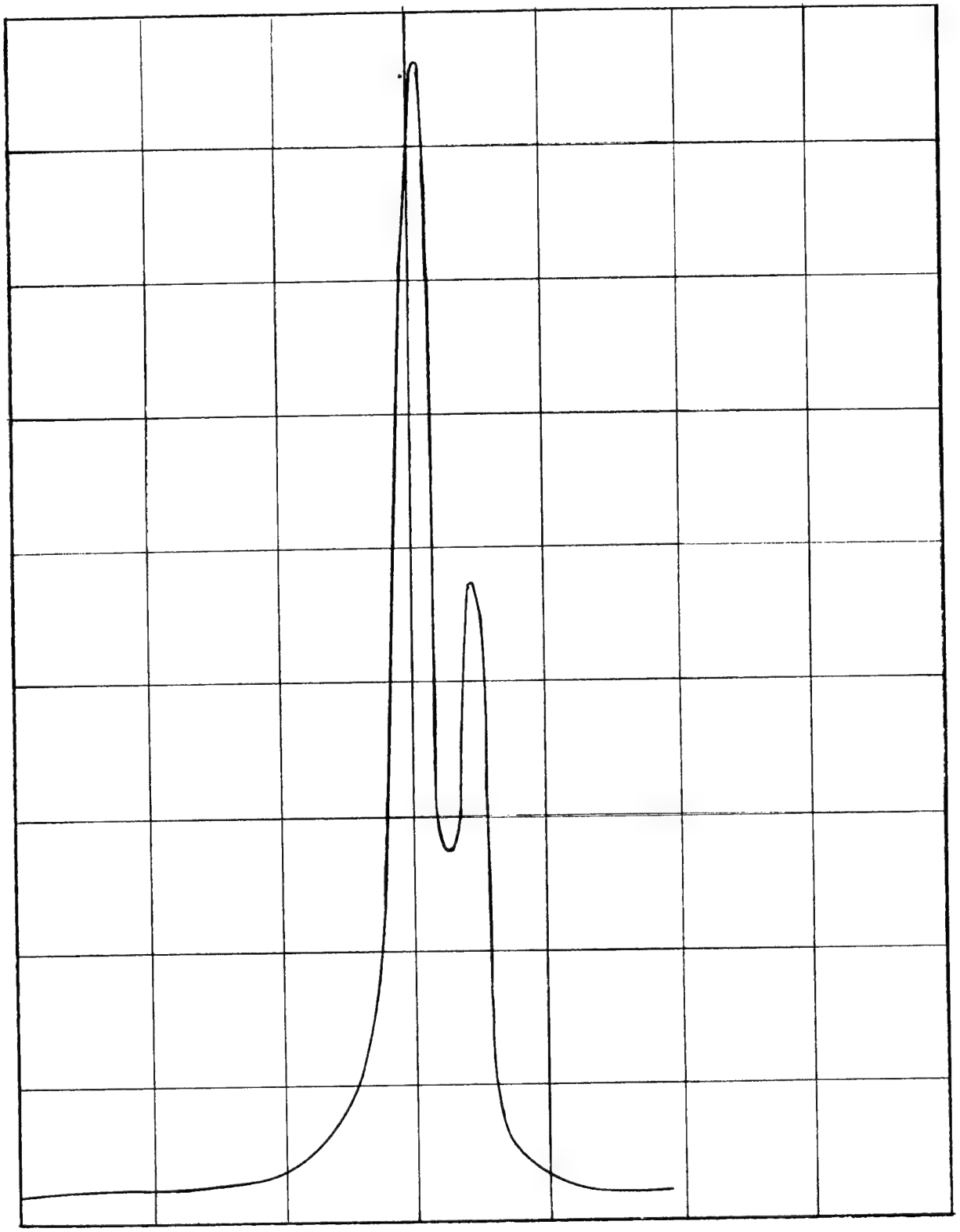

Figure 15. The 200 x-ray diffraction line obtained from pure nickel which has been annealed at 700°C

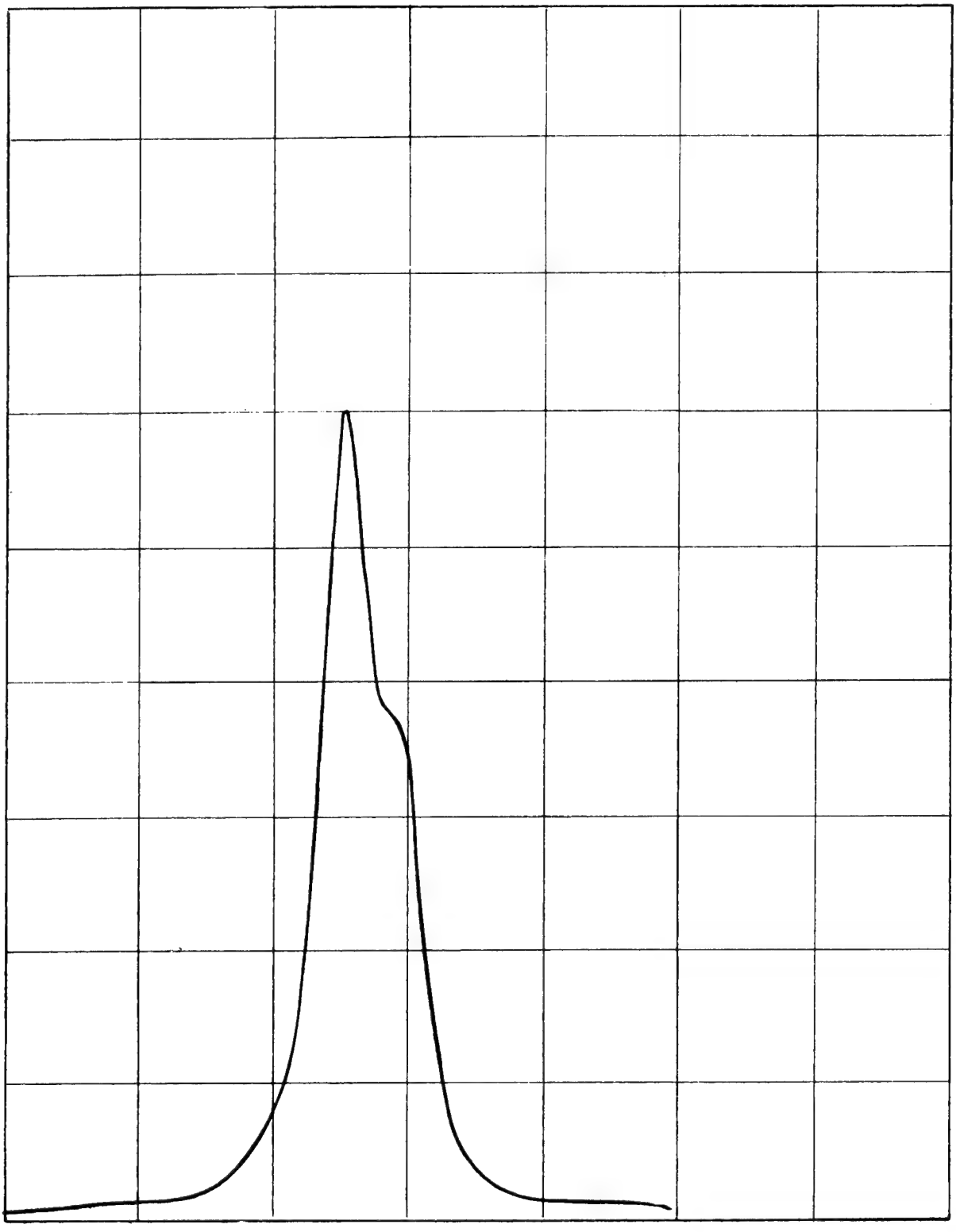

Figure 16. The 200 x-ray diffraction line obtained from TD nickel which has been annealed at 700°C

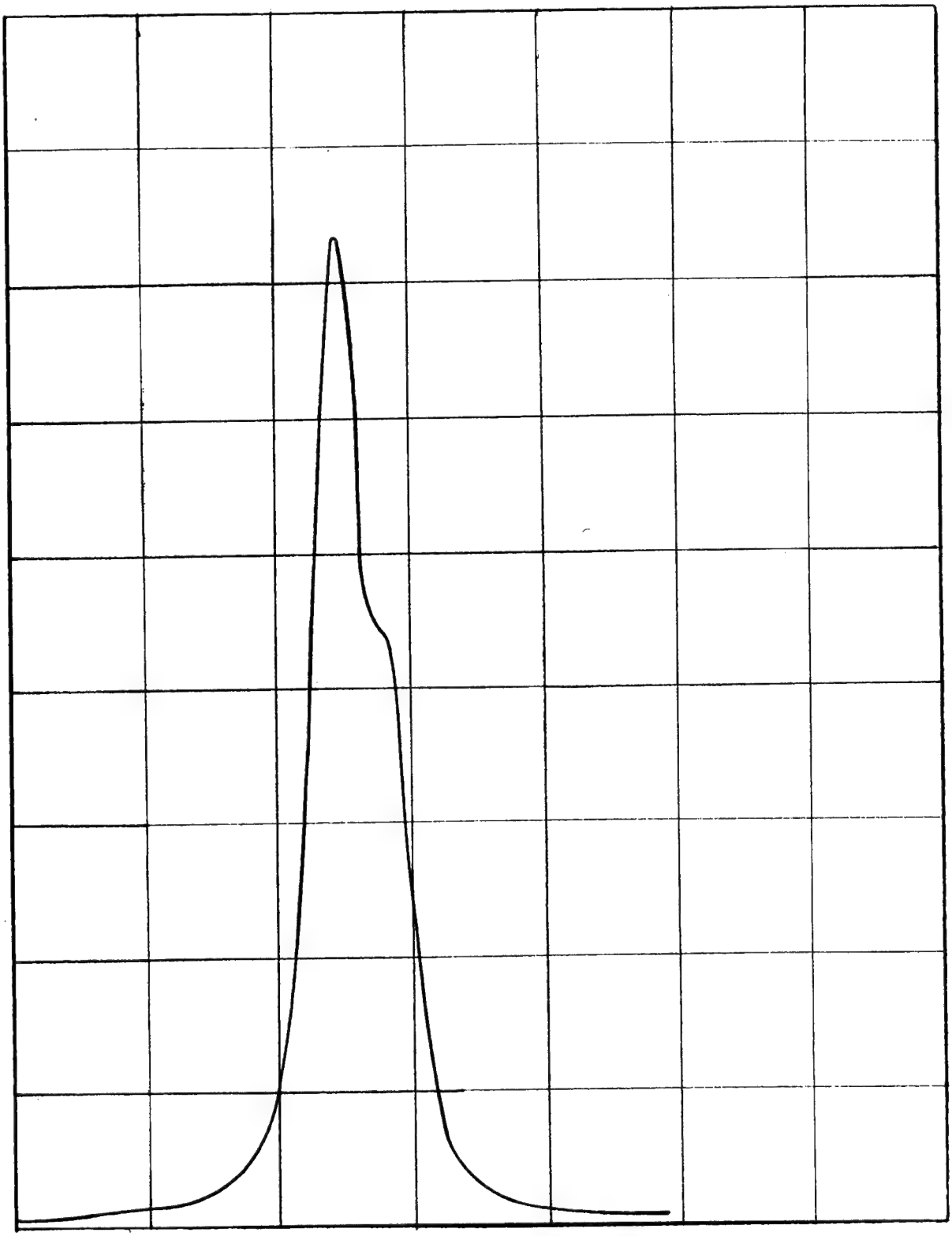

Figure 17. The 200 x-ray diffraction line obtained from TD nickel which has been annealed at 1400°C

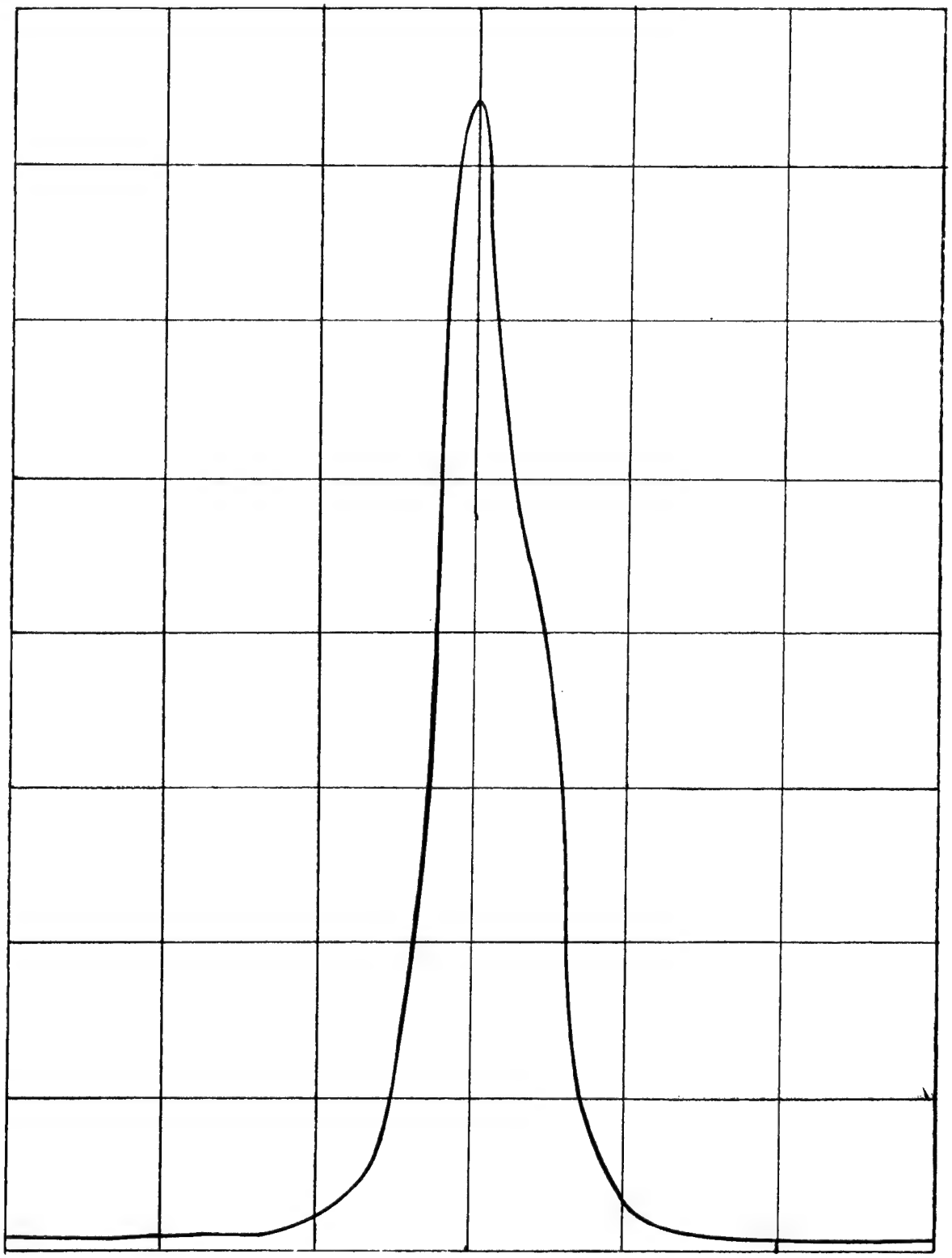

Figure 18. The 200 x-ray diffraction line obtained from TD nickel in the as-received condition

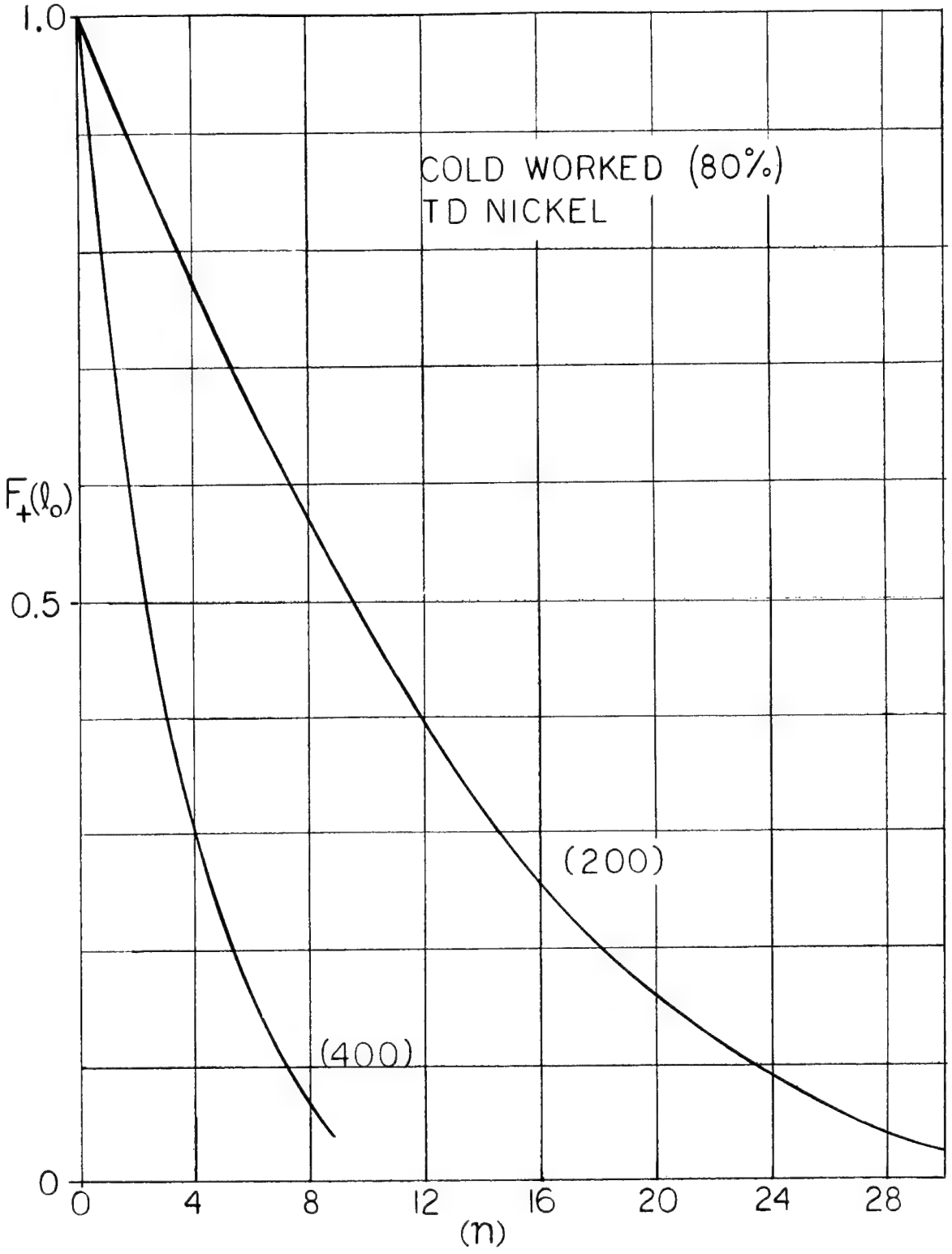

Figure 19. The Fourier coefficients for the 200 and 400 x-ray diffraction lines for cold worked TD nickel

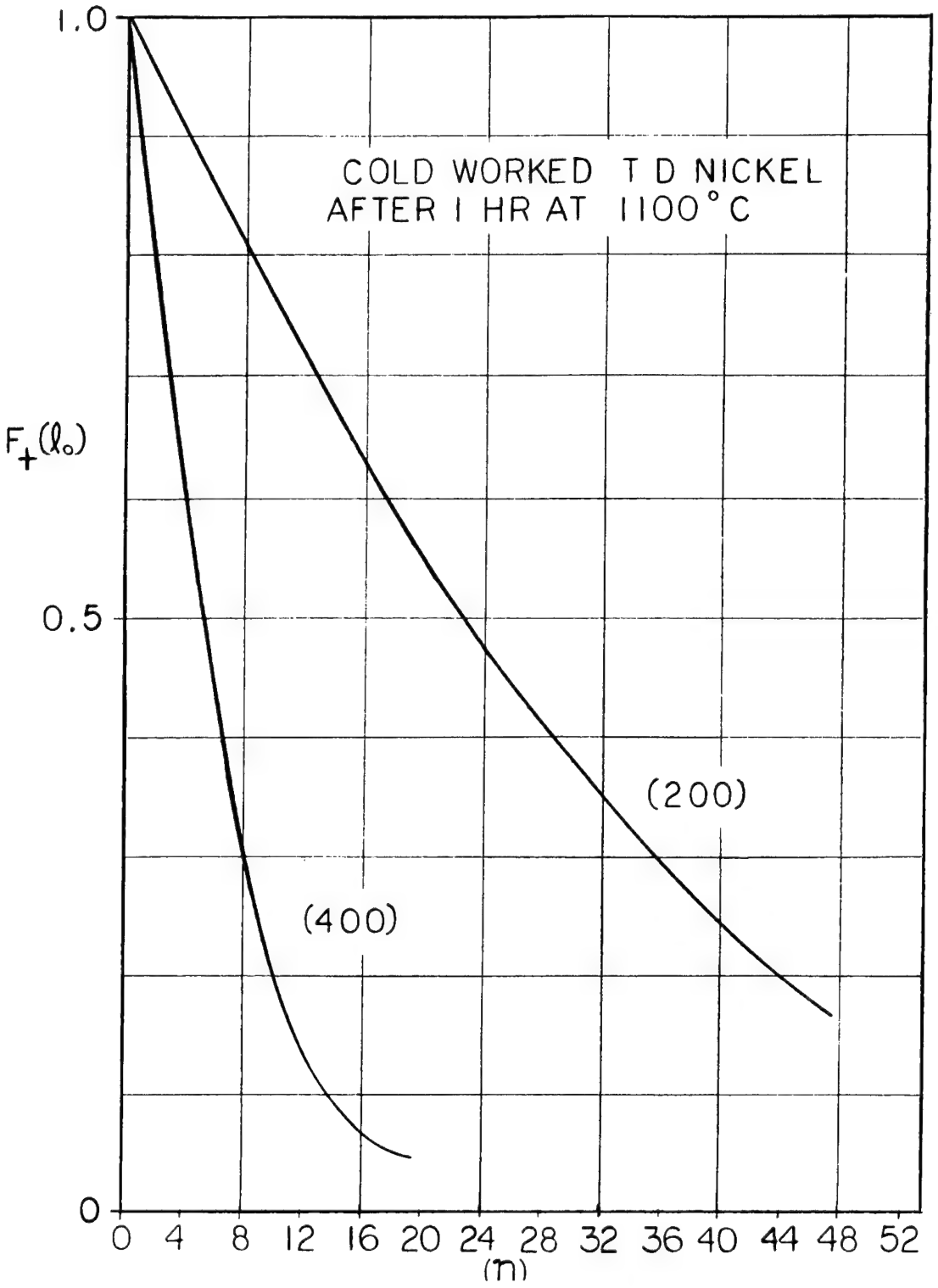

Figure 20. The Fourier coefficients for the 200 and 400 x-ray diffraction lines for TD nickel which has been cold worked and then annealed at 1100°C for 1 hour

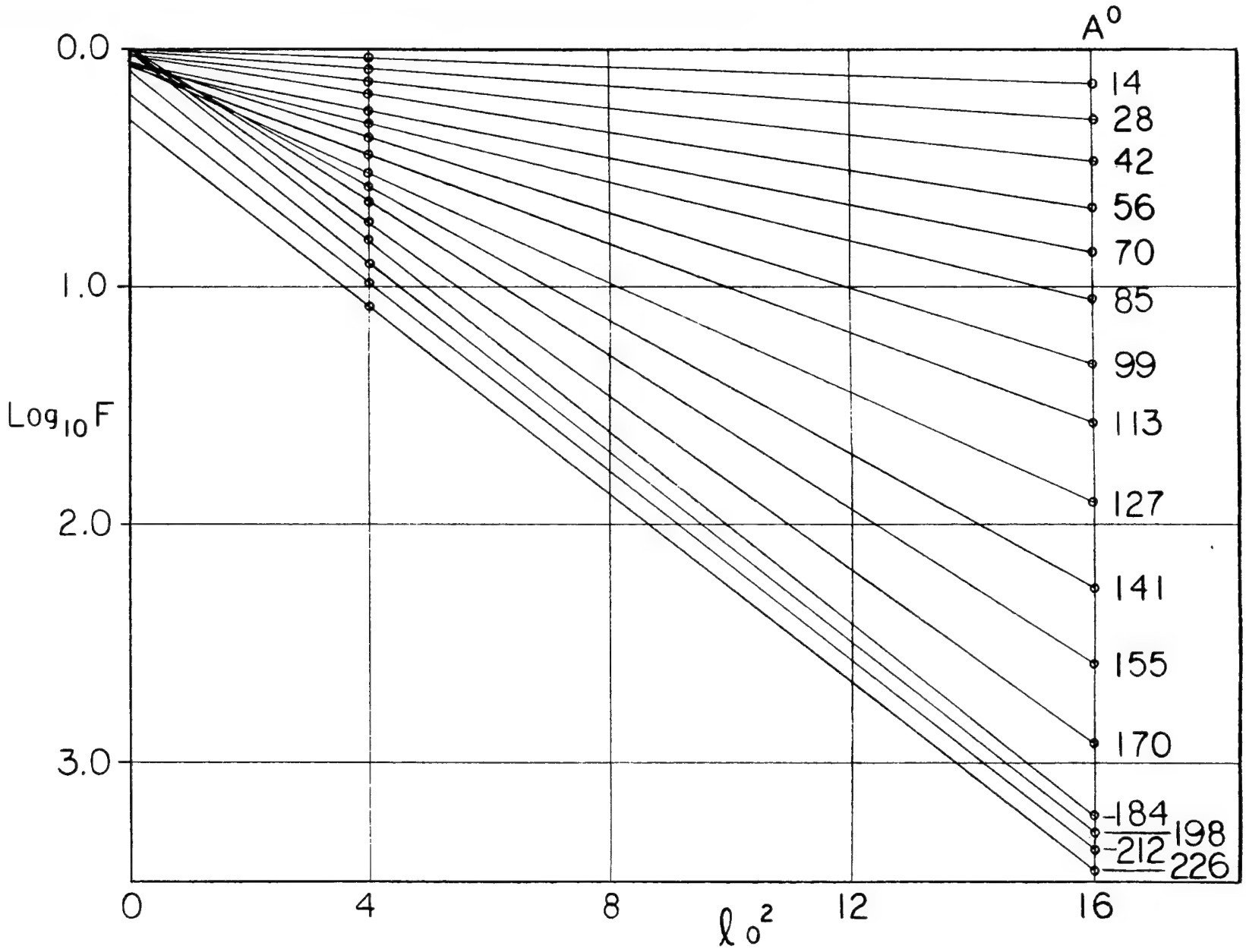

Figure 21. Log $F_t(l_o)$ vs. l_o^2 for TD nickel in the as-received state

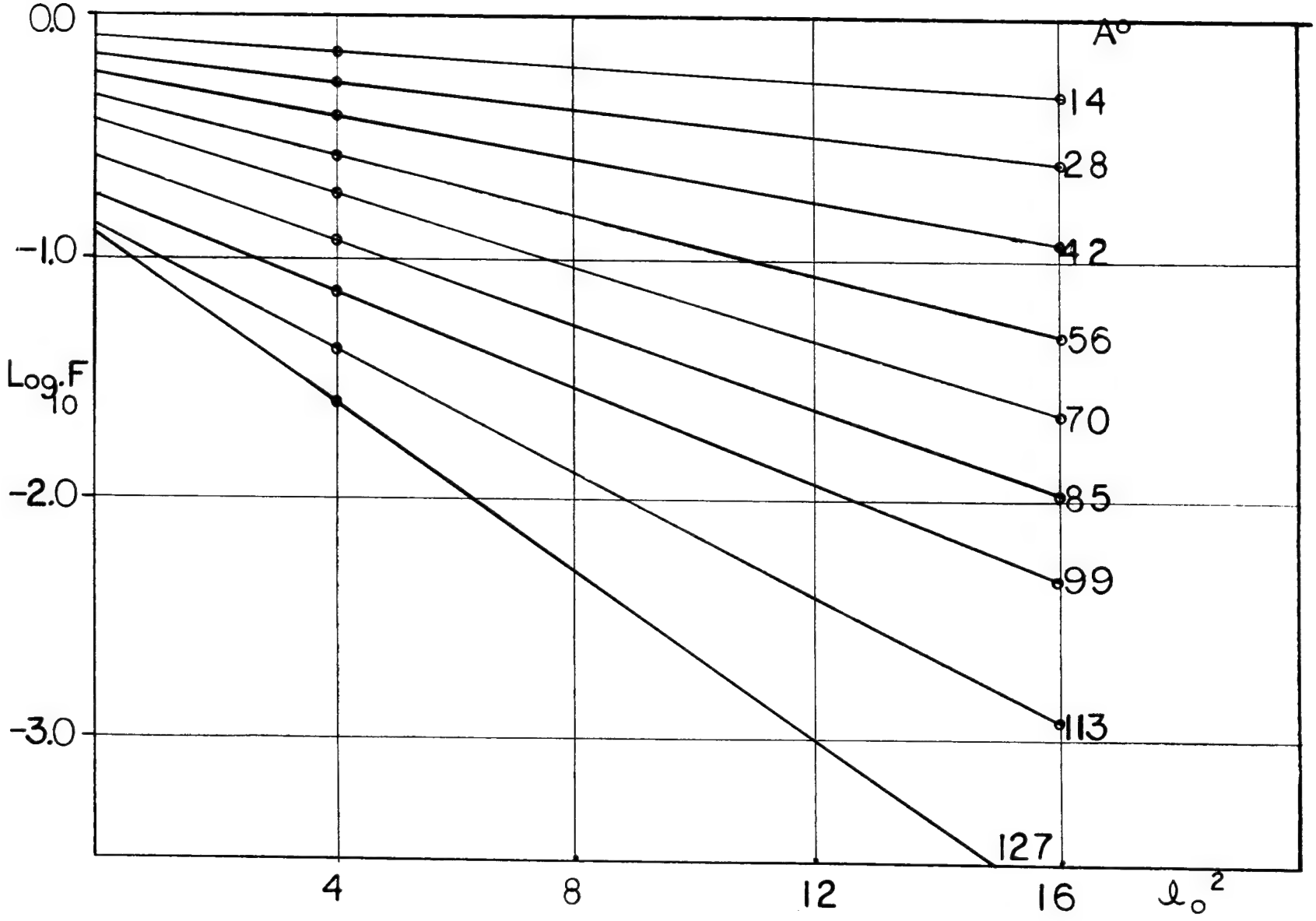

Figure 22. Log $F_t(l_o)$ vs. l_o^2 for cold worked TD nickel

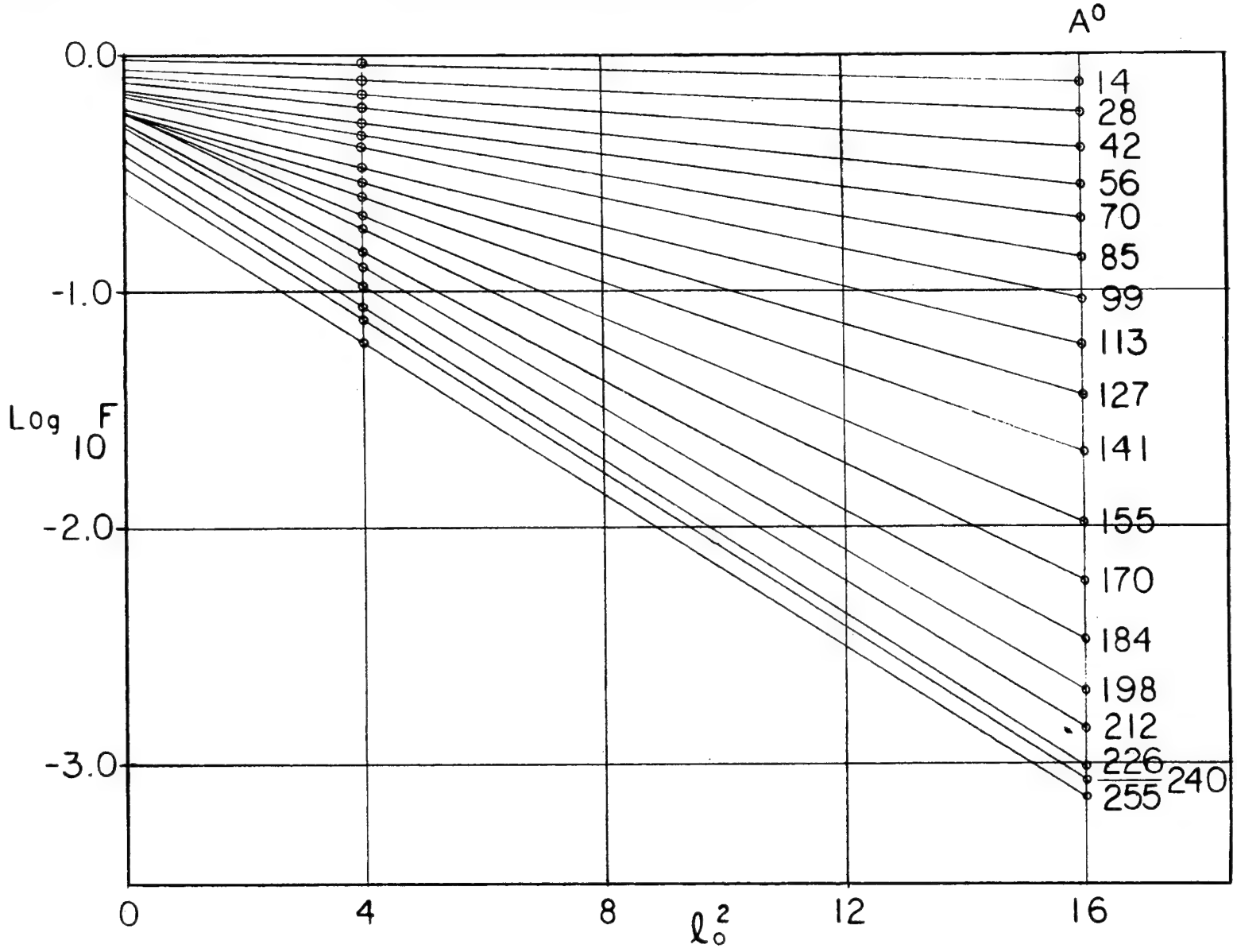

Figure 23. Log $F_t(l_o)$ vs. l_o^2 for TD nickel which has been cold worked and then annealed for 1 hour at 700°C

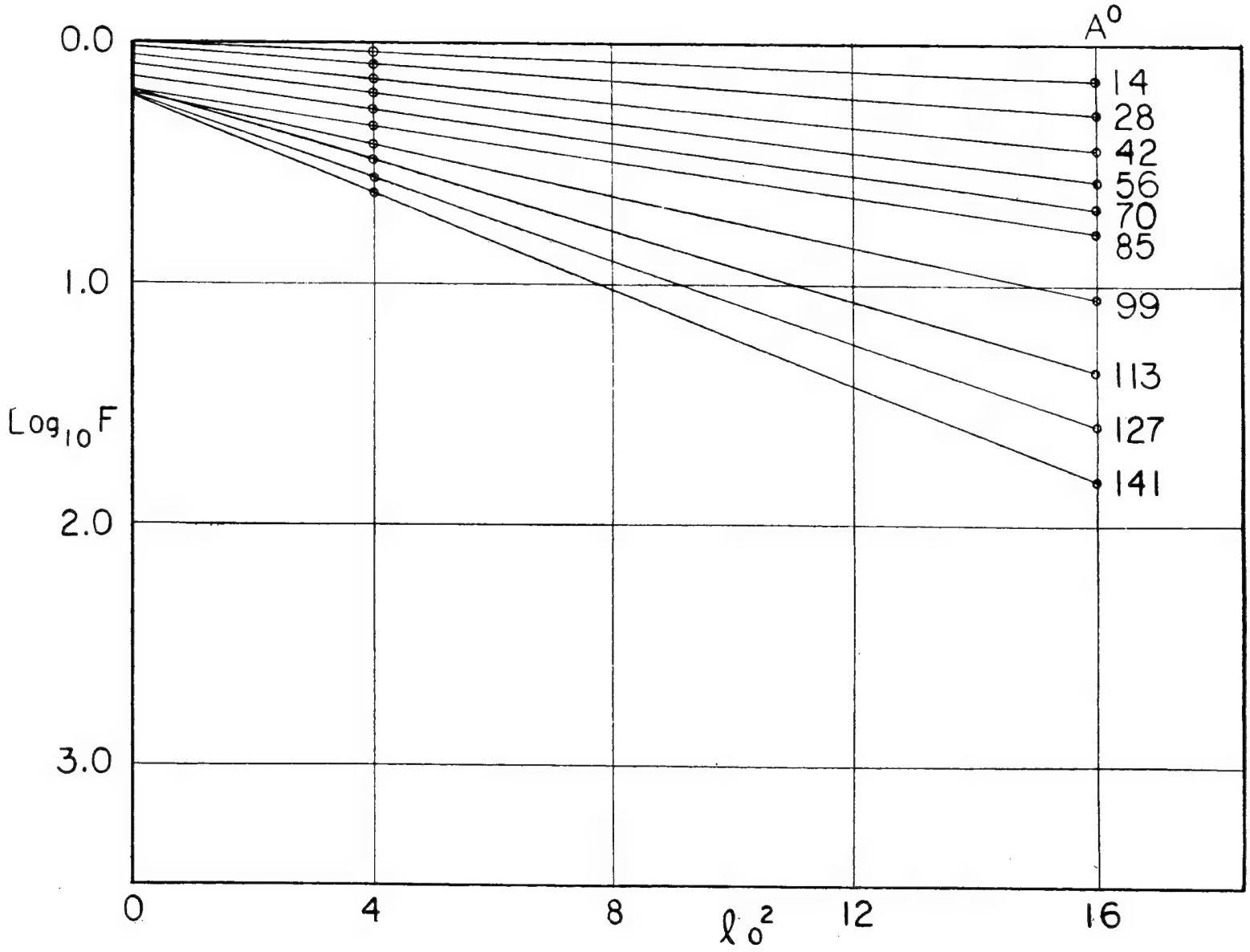

Figure 24. Log F_t (1_o) vs. 1_o^2 for TD nickel which has been cold worked and then annealed for 1 hour at 900°C

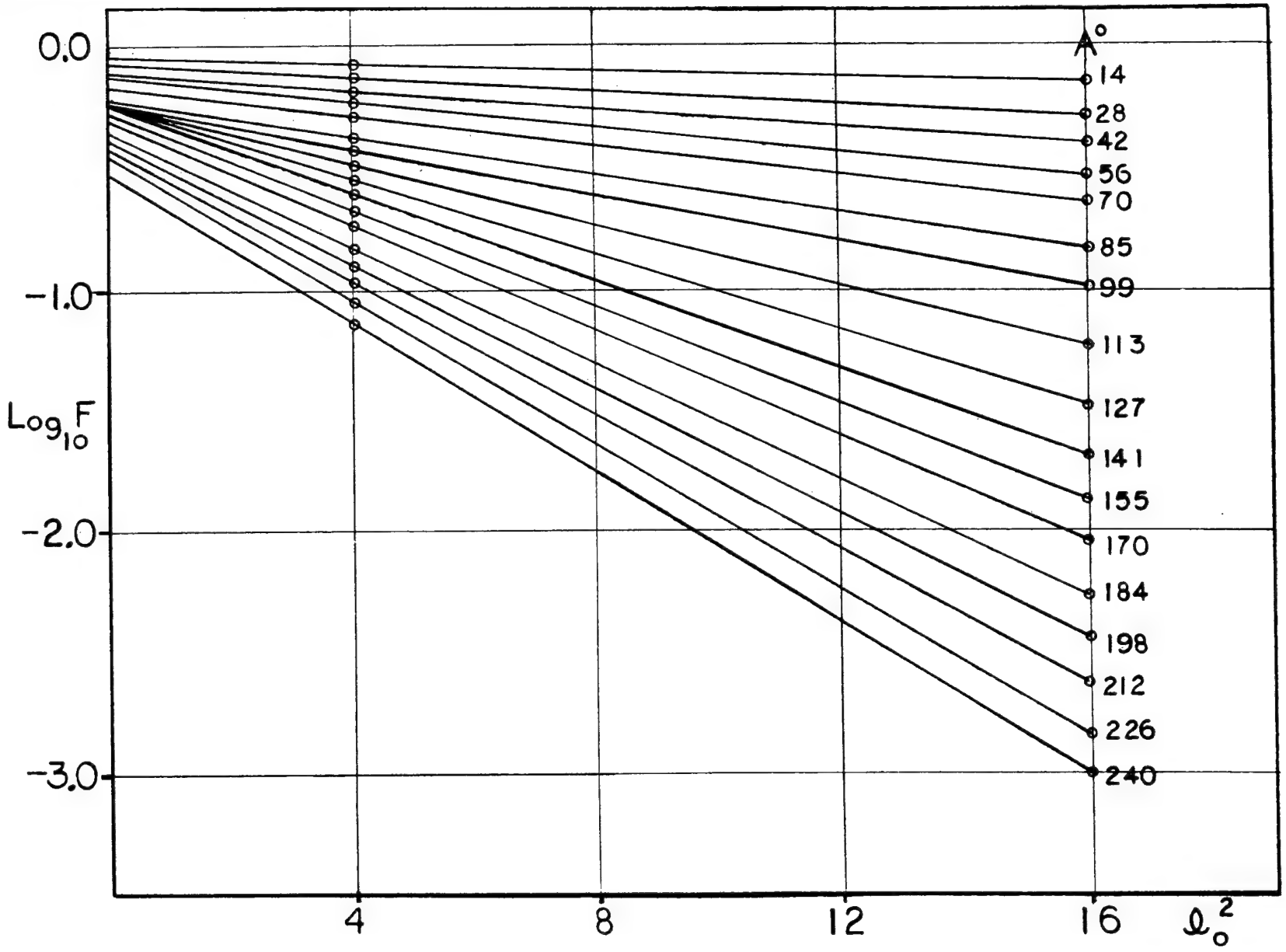

Figure 25. Log F_t (l_o) vs. l_o^2 for TD nickel which has been cold worked and then annealed for 1 hour at 1100°C

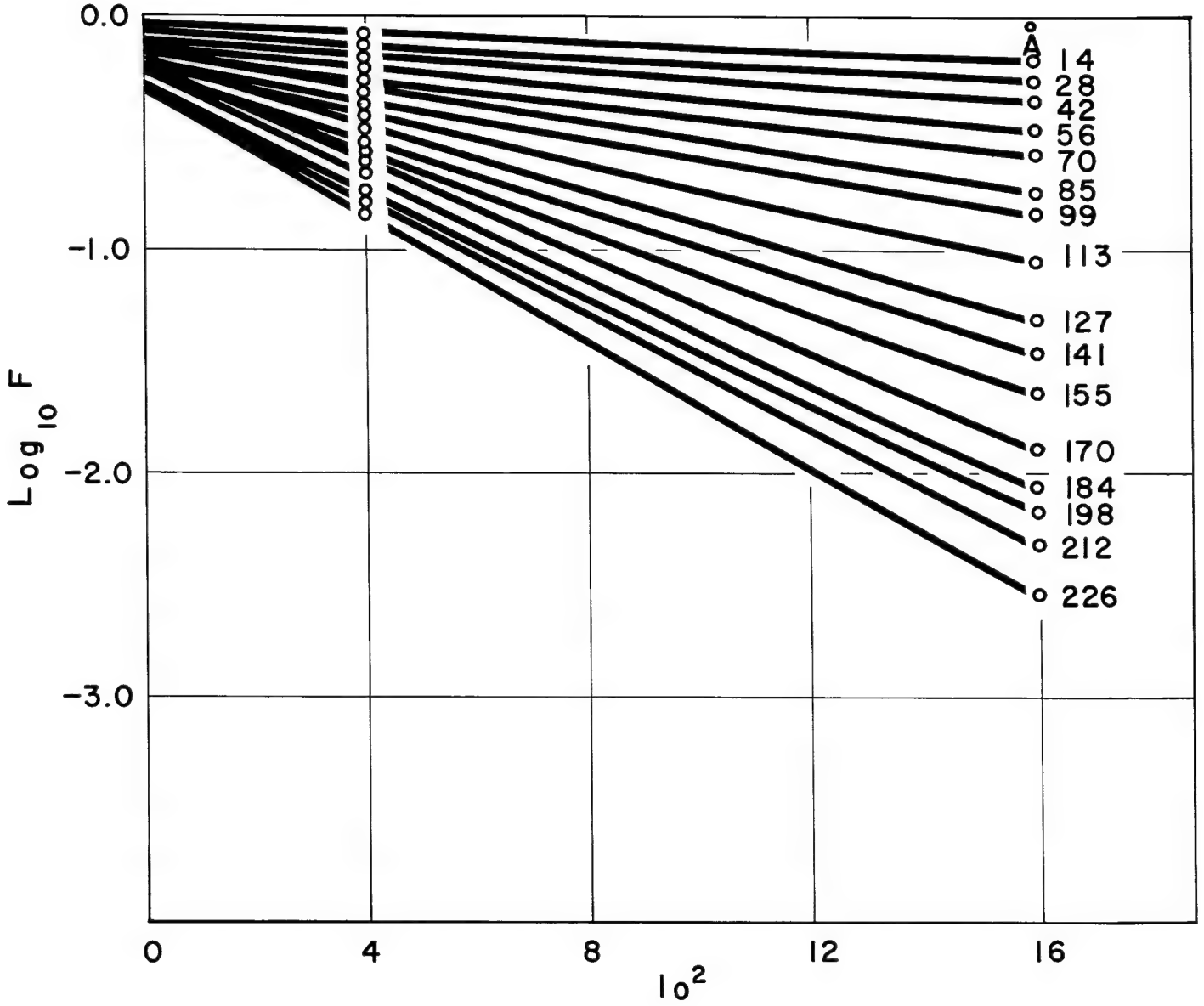

Figure 26. Log F_t (l_o) vs. l_o^2 for TD nickel which has been cold worked and then annealed for 1 hour at 1440°C

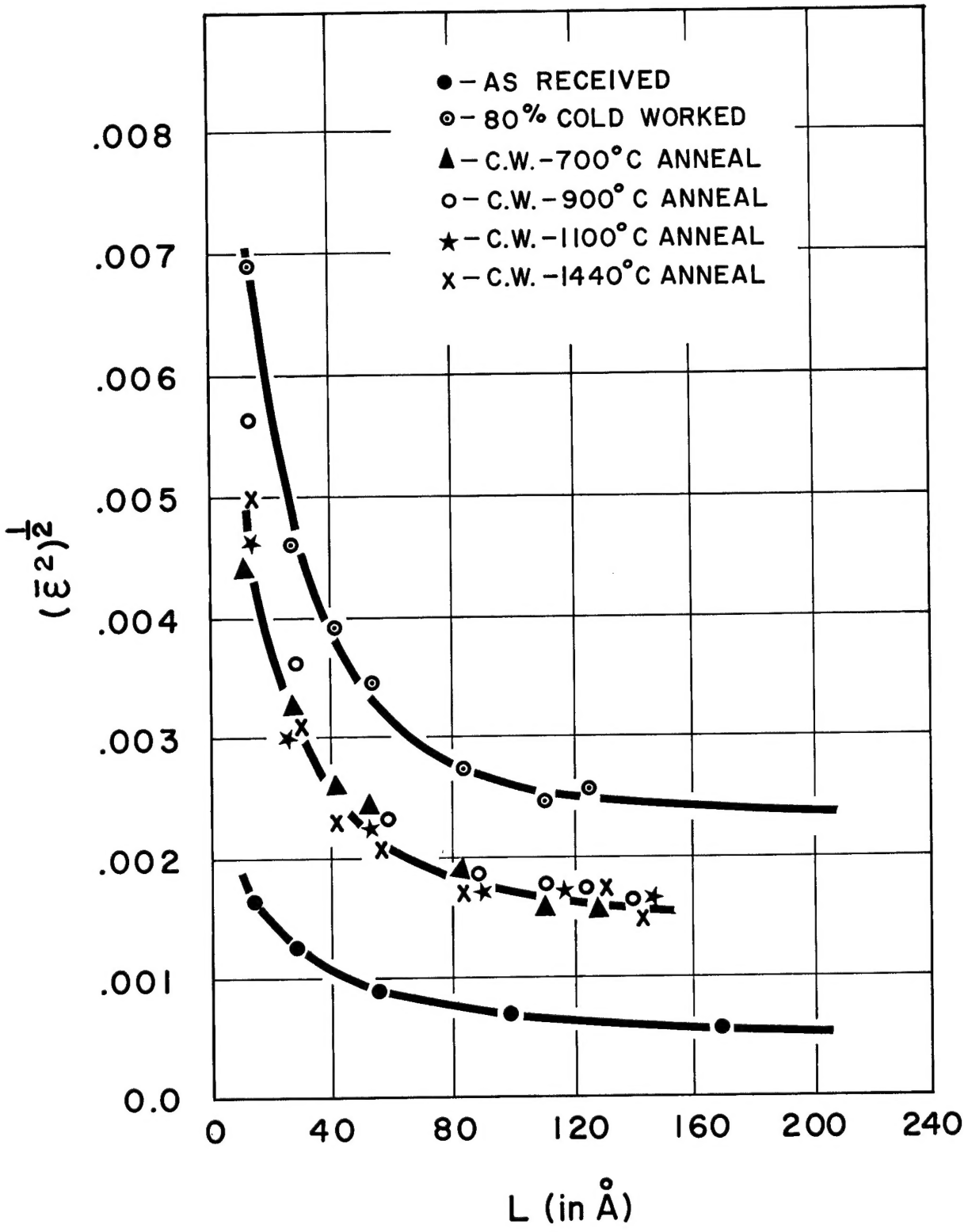

Figure 27. The effect of various heat treatments on the elastic strains in TD nickel

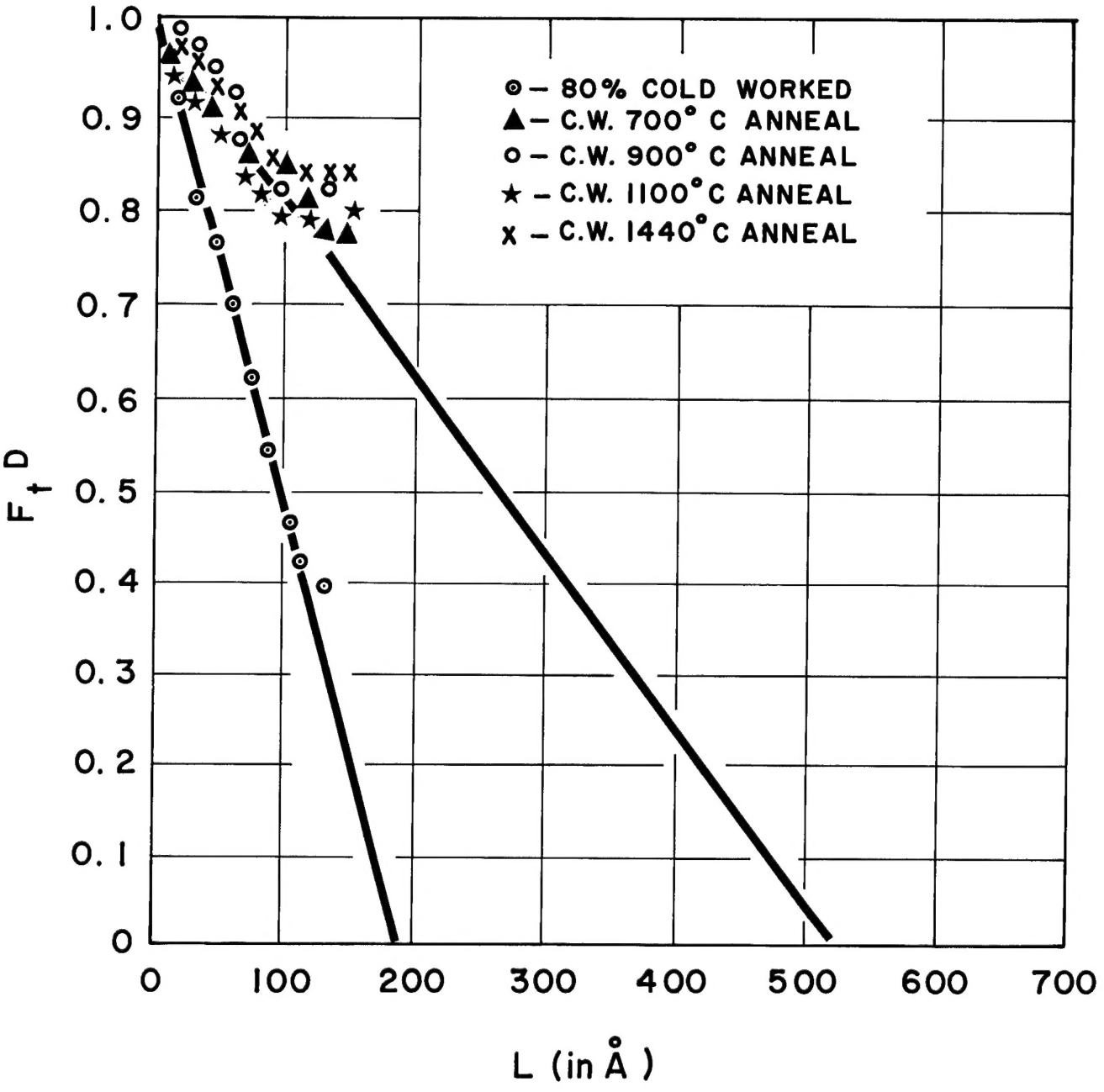

Figure 28. The effect of various heat treatments on the size of the coherently diffracting domains in TD nickel

APPENDIX 1

COMPUTER PROGRAM

```
CALHB
      DIMENSION NSMALH(201),NSMALG(201)
 101  READ 700,(NSMALH(NX),NX=1,201)
 700  FORMAT(14I5)
      IF(NSMALH(1)-99999)701,100,701
 701  READ 800,(NSMALG(NX),NX=1,201)
 800  FORMAT(14I5)
      C= π/50
      DO 500 NT=1,201
      T=NT
      HR=0.
      HI=0.
      GR=0.
      GI=0.
      FR=0.
      FI=0.
      DO 400 NX=1,201
      X=NX-101
      A=COSF(C*X*T)
      B=SINF(C*X*T)
```

Contd...

"The aeronautical and space activities of the United States shall be conducted so as to contribute . . . to the expansion of human knowledge of phenomena in the atmosphere and space. The Administration shall provide for the widest practicable and appropriate dissemination of information concerning its activities and the results thereof."

—NATIONAL AERONAUTICS AND SPACE ACT OF 1958

NASA SCIENTIFIC AND TECHNICAL PUBLICATIONS

TECHNICAL REPORTS: Scientific and technical information considered important, complete, and a lasting contribution to existing knowledge.

TECHNICAL NOTES: Information less broad in scope but nevertheless of importance as a contribution to existing knowledge.

TECHNICAL MEMORANDUMS: Information receiving limited distribution because of preliminary data, security classification, or other reasons.

CONTRACTOR REPORTS: Technical information generated in connection with a NASA contract or grant and released under NASA auspices.

TECHNICAL TRANSLATIONS: Information published in a foreign language considered to merit NASA distribution in English.

TECHNICAL REPRINTS: Information derived from NASA activities and initially published in the form of journal articles.

SPECIAL PUBLICATIONS: Information derived from or of value to NASA activities but not necessarily reporting the results of individual NASA-programmed scientific efforts. Publications include conference proceedings, monographs, data compilations, handbooks, sourcebooks, and special bibliographies.

Details on the availability of these publications may be obtained from:

SCIENTIFIC AND TECHNICAL INFORMATION DIVISION

NATIONAL AERONAUTICS AND SPACE ADMINISTRATION

Washington, D.C. 20546